

ORIGINAL RESEARCH

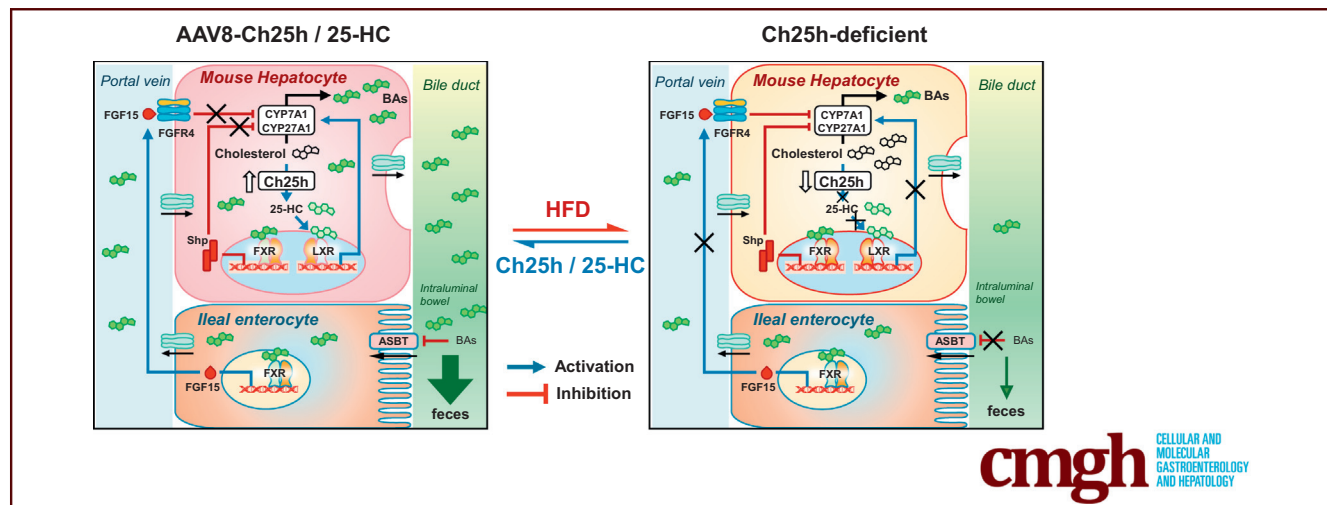


Hepatic Reduction in Cholesterol 25-Hydroxylase Aggravates Diet-induced Steatosis

Zeyu Dong,^{1,*} Fangzhou He,^{1,*} Xiaosong Yan,¹ Yuanming Xing,^{1,2} Yuyang Lei,^{1,2} Jie Gao,^{1,5} Ming He,³ Dongmin Li,⁴ Liang Bai,^{1,2,5,§} Zuyi Yuan,² and John Y-J. Shyy^{1,3,§}

¹Institute of Cardiovascular Science, Translational Medicine Institute, Xi'an Jiaotong University Health Science Center, Xi'an, Shaanxi, China; ²Department of Cardiology, First Affiliated Hospital of Xi'an Jiaotong University, Xi'an, Shaanxi, China;

³Department of Medicine/Division of Cardiology, University of California, San Diego, La Jolla, California; ⁴Department of Genetics and Molecular Biology, Xi'an Jiaotong University Health Science Center, Xi'an, Shaanxi, China; and ⁵Department of Laboratory Animal Science, School of Basic Medical Sciences, Xi'an Jiaotong University, Xi'an, Shaanxi, China



SUMMARY

Hepatic overexpression of cholesterol 25-hydroxylase or exogenous administration of 25-hydroxycholesterol (25-HC) in mice drastically reduced the high-fat diet-induced hepatic steatosis via massive production of bile acids. The underlying mechanism involves 25-HC activation of the liver X receptor-cytochrome P450 7A1 pathway.

BACKGROUND & AIMS: Cholesterol 25-hydroxylase (Ch25h), converting cholesterol to 25-hydroxycholesterol (25-HC), is critical in modulating cellular lipid metabolism and anti-inflammatory and antiviral activities. However, its role in nonalcoholic fatty liver disease remains unclear.

METHODS: Ch25h expression was detected in livers of ob/ob mice and E3 rats fed a high-fat diet (HFD). Gain- or loss-of-function of Ch25h was performed using Ch25h^{+/+} (wild type [WT]) mice receiving AAV8-Ch25h or Ch25h knockout (Ch25h^{-/-}) mice. WT mice fed an HFD were administered with 25-HC. The Ch25h-LXR α -CYP axis was measured in primary hepatocytes isolated from WT and Ch25h^{-/-} mice.

RESULTS: We found that Ch25h level was decreased in livers of ob/ob mice and E3 rats fed an HFD. Ch25h^{-/-} mice fed an HFD showed aggravated fatty liver and decreased level of cytochrome P450 7A1 (CYP7A1), in comparison with their WT littermates. RNA-seq analysis revealed that the differentially expressed genes in livers of HFD-fed Ch25h^{-/-} mice were involved in pathways of positive regulation of lipid metabolic process, steroid metabolic process, cholesterol metabolic process, and bile acid biosynthetic process. As gain-of-function experiments, WT mice receiving AAV8-Ch25h or 25-HC showed alleviated NAFLD, when compared with the control group receiving AAV8-control or vehicle control. Consistently, Ch25h overexpression significantly elevated the levels of primary and secondary bile acids and CYP7A1 but decreased those of small heterodimer partner and FGFR4.

CONCLUSIONS: Elevated levels of Ch25h and its enzymatic product 25-HC alleviate HFD-induced hepatic steatosis via regulating enterohepatic circulation of bile acids. The underlying mechanism involves 25-HC activation of CYP7A1 via liver X receptor. These data suggest that targeting Ch25h or 25-HC may have therapeutic advantages against nonalcoholic fatty liver disease. (*Cell Mol Gastroenterol Hepatol* 2022;13:1161-1179; <https://doi.org/10.1016/j.jcmgh.2021.12.018>)

Keywords: 25-HC; Bile Acid Metabolism; Ch25h; CYP7A1; Hepatic Steatosis.

See editorial on page 1265.

Nonalcoholic fatty liver disease (NAFLD) is closely associated with obesity, diabetes, dyslipidemia, and atherosclerosis. As the most common chronic liver disease, persistent NAFLD can progress to nonalcoholic steatohepatitis and end-stage liver diseases such as cirrhosis and hepatocellular carcinoma.¹ Effective prevention and therapy for NAFLD remain elusive,² which highlights the unmet need for understanding the molecular mechanisms and new therapeutic strategies for this disease.

Homeostatic conversion of cholesterol to bile acids (eg, cholic acid [CA] and chenodeoxycholic acid [CDCA]) is the primary pathway for cholesterol catabolism, but accumulation of free cholesterol in the liver contributes to the pathogenesis of NAFLD.^{3,4} Cytochrome P450 7A1 (CYP7A1), a liver-specific enzyme, catalyzes the first and rate-limiting step of bile acid biosynthesis. Bile acid metabolism at the systems level is under tight control of enterohepatic circulation.⁵ In the rodent liver, CYP7A1 is transcriptionally upregulated by the nuclear receptor liver X receptor α (LXR α), a nuclear receptor governing oxysterol metabolism.^{6,7} Bile acids facilitate fat absorption by enterocytes. However, most bile acids are reabsorbed in the ileum and circulate back to the liver via portal circulation to inhibit CYP7A1 and thereby prevent excessive production of bile acids.⁸ This feedback inhibition of bile acid synthesis is mediated by fibroblast growth factor 15 (FGF15)/19 in the ileum and small heterodimer partner (Shp) in the liver, both regulated by the axis bile acid–farnesoid X receptor (FXR).^{9,10}

Ample evidence indicates that bile acid metabolism plays a critical role in the development of NAFLD. Transgenic mice overexpressing CYP7A1 are resistant to high-fat diet (HFD)-induced obesity and fatty liver via increased CYP7A1 expression and enlarged bile acid pool.^{11,12} Administration of CA and ursodeoxycholic acid (UDCA) to ob/ob mice markedly improved hepatic steatosis.¹³ Similarly, administration of fatty acid-bile acid conjugates to HFD-fed rodent models alleviated NAFLD.¹⁴ However, whether CYP7A1 ablation is beneficial or detrimental is still debated, as Ferrell et al showed that CYP7A1 $^{-/-}$ mice are protected against HFD/high-cholesterol diet-induced metabolic disorders.¹⁵

Cholesterol 25-hydroxylase (Ch25h), catalyzing the hydroxylation of cholesterol to 25-hydroxycholesterol (25-HC), plays an important role in cholesterol and lipid metabolism.^{16,17} Acting as an endogenous ligand of LXR, 25-HC positively affects the expression of cholesterol catabolism-related genes, including ABCA1 and ABCG1.¹⁶ However, 25-HC negatively regulates sterol regulatory element-binding protein 2 (SREBP2), the key transcription factor regulating cholesterol metabolism.¹⁸ At an ample cellular level, 25-HC inhibits SREBP2 activity by sandwiching itself between Scap and Insig-2,¹⁹ thereby sequestering the Scap-SREBP2 complex on the ER membrane. In addition to

its regulation of cholesterol metabolism, Ch25h is an interferon-stimulated gene with antiviral activity against various enveloped viruses, including severe acute respiratory syndrome coronavirus 2.^{20,21} With respect to hepatic metabolism, hepatic overexpression of Ch25h in mice improved glucose tolerance and insulin sensitivity.²²

The purpose of this study was to examine whether hepatic augmentation of Ch25h could ameliorate NAFLD. Using mouse models with gain- and loss-of-function of Ch25h, we found that the hepatic upregulation of Ch25h or exogenous administration of 25-HC greatly reduced HFD-induced hepatic steatosis via massive production of bile acids. These results reveal a beneficial role of Ch25h and 25-HC in regulating cholesterol catabolism in the liver and a potential strategy for NAFLD therapy.

Results

Ch25h Expression is Decreased in Fatty Liver

Obese ob/ob mice and E3 rats fed an HFD exhibit NAFLD.^{23,24} To determine whether a change in Ch25h level is involved in these NAFLD rodent models, we first compared the expression of Ch25h in livers of ob/ob mice and wild-type (WT) littermate controls. Hepatic mRNA and protein levels of Ch25h were significantly decreased in ob/ob mice as compared with WT mice (Figure 1A and 1E). As well, LXR α , CYP7A1, and CYP27A1 expression were decreased (Figure 1B–1E). In contrast, SREBP1 and SREBP2 mRNA levels were increased in livers of ob/ob mice (Figure 1F and 1G). Similar decreases in mRNA levels of Ch25h, LXR α , CYP7A1, and CYP27A1 were found in livers of E3 rats fed an HFD than control rats under a chow diet (Figure 1H–1K). Because 25-HC is a ligand of LXR α and LXR α transactivates CYP7A1 and CYP27A1,⁶ we validated the hierarchical regulation of the Ch25h-LXR α -CYP axis by using primary hepatocytes isolated from WT, Ch25h-deficient, or overexpression mice. Ch25h deficiency in mouse hepatocytes increased

*Authors share co-first authorship; §Authors share co-senior authorship.

Abbreviations used in this paper: 25-HC, 25-hydroxycholesterol; ASBT, apical sodium-dependent bile acid transporter; CA, cholic acid; CDCA, chenodeoxycholic acid; Ch25h, cholesterol 25-hydroxylase; CYP7A1, cytochrome P450 7A1; DCA, deoxycholic acid; DEGs, differentially expressed genes; FGF15, fibroblast growth factor 15; FXR, farnesoid X receptor; GO, Gene Ontology; HDCA, α -hyodeoxycholic acid; HDL-C, high-density lipoprotein cholesterol; HFD, high-fat diet; IL, interleukin; LCA, lithocholic acid; LDL-C, low-density lipoprotein cholesterol; LXR, liver X receptor; MCP-1, monocyte chemoattractant protein 1; NAFLD, non-alcoholic fatty liver disease; qPCR, quantitative polymerase chain reaction; Shp, small heterodimer partner; SREBP2, sterol regulatory element-binding protein 2; TC, total cholesterol; TCA, taurocholic acid; TCDCA, taurochenodeoxycholate; TDCA, taurodeoxycholate; TG, triglyceride; THDCA, taurohyodeoxycholic acid; TNF α , tumor necrosis factor α ; TUDCA, taurooursodeoxycholic acid; T α MCA, taur α -muricholate; T β MCA, taur β -muricholate; T ω MCA, taur ω -muricholate; UDCA, ursodeoxycholic acid; VLDL, very low-density lipoprotein; WT, wild-type; α MCA, α -muricholic acid; β MCA, β -muricholic acid; ω MCA, ω -muricholic acid.

Most current article

© 2022 The Authors. Published by Elsevier Inc. on behalf of the AGA Institute. This is an open access article under the CC BY-NC-ND license (<http://creativecommons.org/licenses/by-nc-nd/4.0/>).

2352-345X

<https://doi.org/10.1016/j.jcmgh.2021.12.018>

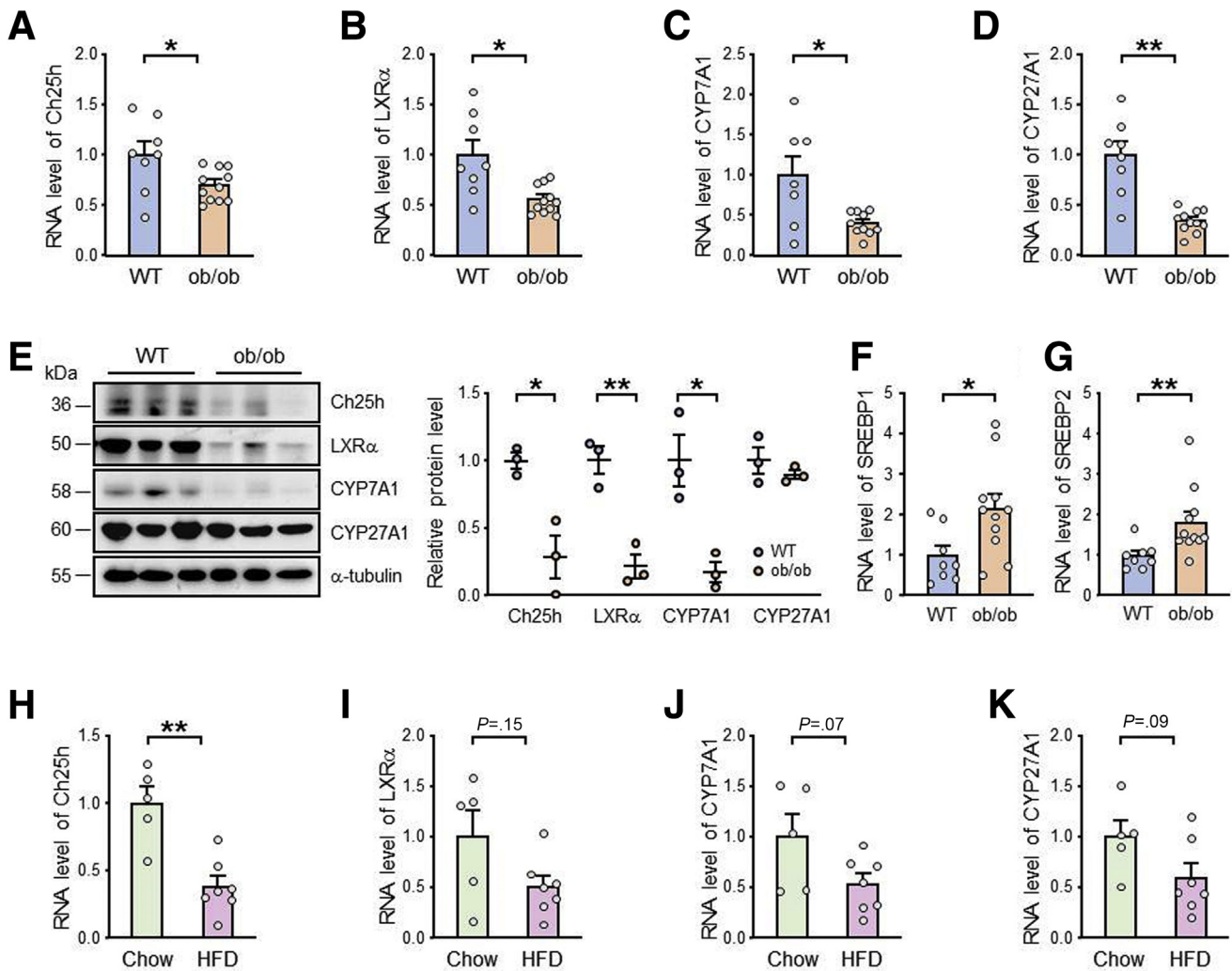


Figure 1. Ch25h expression is decreased in liver of obese rodent animals. RT-qPCR analysis of mRNA levels of Ch25h (A), LXR α (B), CYP7A1 (C), CYP27A1 (D), SREBP1 (F), and SREBP2 (G) in livers of 6 month-old C57BL/6J mice (WT) ($n = 8$) and ob/ob mice ($n = 11$). (E) Western blot analysis of protein levels of Ch25h, LXR α , CYP7A1, and CYP27A1 in livers of WT and ob/ob mice ($n = 3$ mice/group). RT-qPCR analysis of mRNA levels of Ch25h (H), LXR α (I), CYP7A1 (J), and CYP27A1 (K) in livers of E3 rats fed a chow diet ($n = 5$) or HFD ($n = 7$) for 12 weeks. Data are presented as mean \pm standard error of the mean. Significance for data in (A–F) and (H–K) was determined by the Student 2-tailed *t* test and those in (G) by the Mann-Whitney *U* test. **P* < .05; ***P* < .01.

mRNA expression of CYP7A1 and CYP27A1, whereas it decreased the protein levels of CYP7A1, but not CYP27A1 (Figure 2A–2C). Conversely, overexpression of Ch25h in WT hepatocytes increased the protein level of CYP7A1, which was blocked by treatment of GSK2033, a LXR α antagonist (Figure 2D). These results demonstrate that Ch25h activates CYP7A1 in rodent hepatocytes.

Ch25h Deficiency Promotes HFD-induced Hepatic Steatosis

Because of the decreased level of Ch25h in livers of obese rodent models and reduced level of CYP7A1 in Ch25h-deficient mouse hepatocytes, we inferred a causal effect of Ch25h loss on hepatic steatosis. Accordingly, Ch25h $^{-/-}$ mice and their WT littermates were fed an HFD or chow diet.

Compared with WT mice, Ch25h $^{-/-}$ mice showed comparable body weight under chow diet, but elevated body weight after HFD feeding for 8 weeks (data not shown). Macroscopically, HFD feeding induced hepatic macrovesicular steatosis in both Ch25h $^{-/-}$ and WT mice (Figure 3A). However, livers of Ch25h $^{-/-}$ mice were more enlarged and paler than WT mice (Figure 3A), with greater liver weight (Figure 3B) and liver weight-to-body weight ratio (Figure 3C). Hepatic lipid accumulation and steatosis were substantial in Ch25h $^{-/-}$ mice, as revealed by hematoxylin and eosin staining, steatosis score, and Oil-red O staining (Figure 3D–3F). Among the 4 groups of mice, Ch25h $^{-/-}$ mice showed the most elevated hepatic levels of total cholesterol (TC) and triglyceride (TG) and circulatory level of low-density lipoprotein cholesterol (LDL-C) (Figure 3G–3J). Furthermore, we performed quantitative polymerase chain reaction (qPCR)

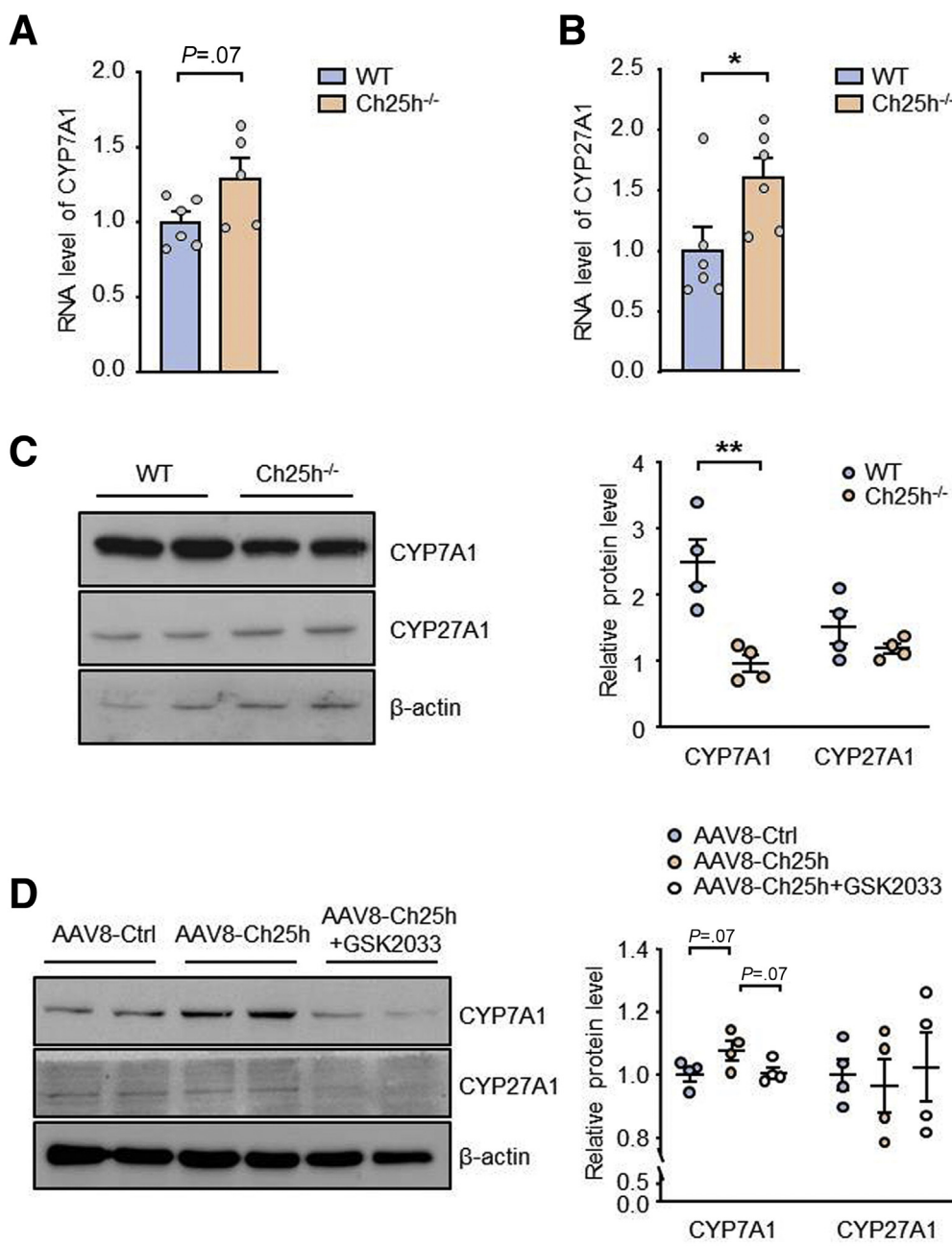


Figure 2. Ch25h activation of CYP7A1 via LXR α . RT-qPCR analysis of mRNA levels of CYP7A1 (A) and CYP27A1 (B) in cultured primary hepatocytes from WT and Ch25h^{-/-} mice. (C) Western blot analysis of protein levels of CYP7A1 and CYP27A1. (C) Western blot analysis was performed to show the protein level of CYP7A1 and CYP27A1 in cultured primary hepatocytes isolated from AAV8-control or AAV8-Ch25h-injected mice ($n = 3$ mice/group), along with treated with or without LXR α antagonist (GSK2033) for 24 hours. Data are presented as mean \pm standard error of the mean. For data in (A) and (C), significance was determined by the Student 2-tailed *t* test. For data in (B), significance was determined by the Mann-Whitney *U* test. For data in (D), significance was determined by the 1-way analysis of variance test between multiple groups. * $P < .05$; ** $P < .01$.

analysis to assess mRNA levels of lipid metabolic genes in livers of WT and Ch25h^{-/-} mice under HFD. SREBP1c, FASN, and Fabp4 were remarkably increased in Ch25h^{-/-} mice as compared with WT mice (Figure 3J). By contrast, the levels of mRNA for fatty acid β -oxidation, including Cpt1, Cpt2, Ascl1, and Acadl, were significantly decreased in Ch25h^{-/-} mice (Figure 3K). There were little changes in hepatic mRNA levels of genes involved in very low-density lipoprotein (VLDL) secretion (ApoB, Mttp) (Figure 3L). However, VLDL secretion was slightly decreased in Ch25h^{-/-} mice as compared with WT mice after injection of Tyloxapol, corresponding to the increased level of plasma TG (Figure 3M).

Together, the results in Figures 1 to 3 suggest that Ch25h attenuation is associated with NAFLD in rodent models.

Ch25h Deficiency Alters Bile Acid Metabolism

To investigate how Ch25h deficiency aggravated the HFD-induced hepatic steatosis, we used RNA-seq analysis of liver tissues from the 4 groups of mice. Principal component analysis shown in Figure 4A indicates that gene expression profiles in these 4 groups clearly varied, as indicated by the first and second eigenvectors. Next, differentially expressed genes (DEGs) (\log_2 fold change >0.5 ; $P < .05$) between WT

and Ch25h^{-/-} mice fed a chow diet or HFD were selected for Gene Ontology (GO) analysis. With reference to WT livers, livers of Ch25h^{-/-} mice under a chow diet showed

enrichment of genes involved in pathways of epoxygenase P450 (GO:0019373), defense response to virus (GO:0051607), and innate immune response (GO:0045087)

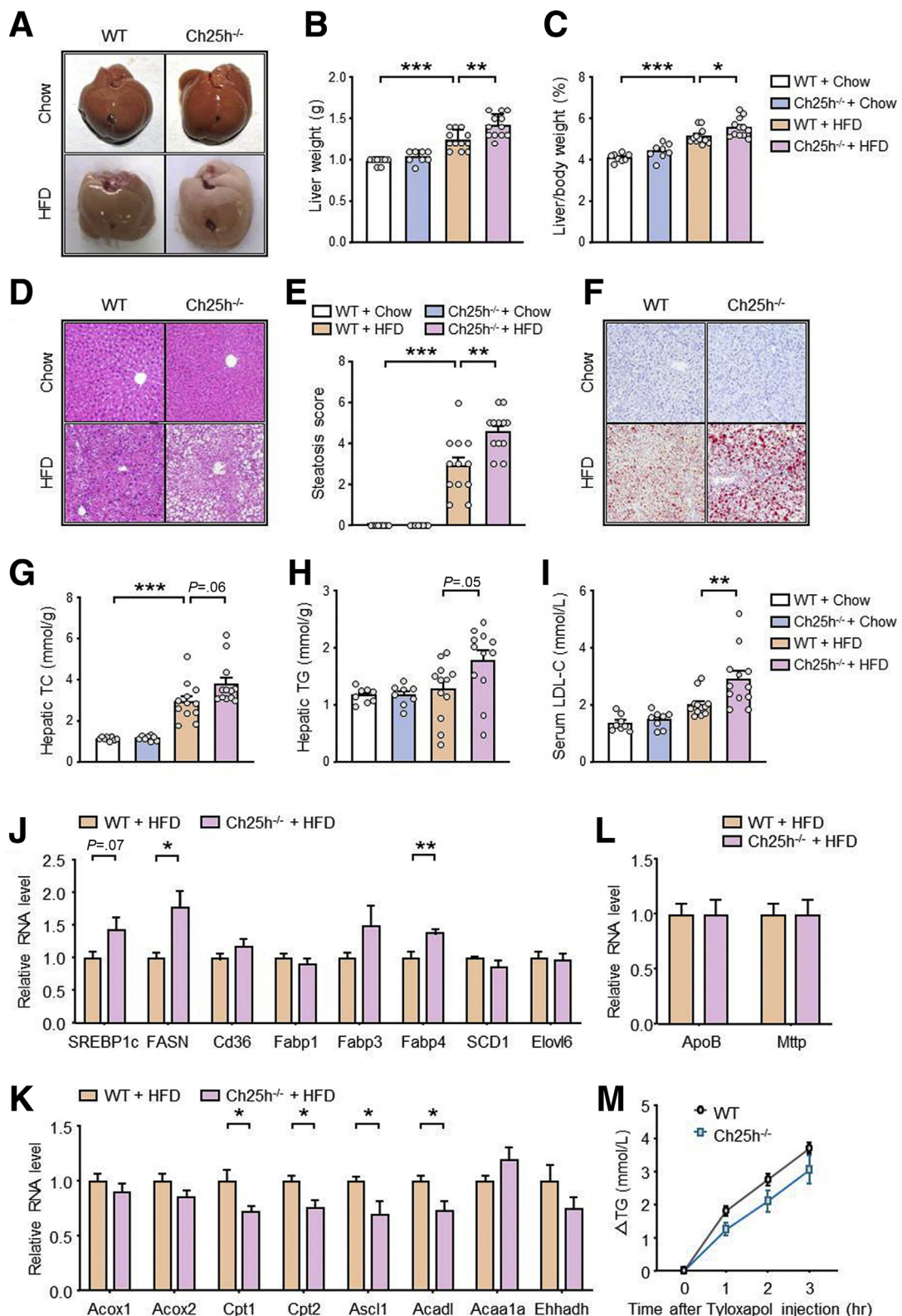


(Figure 4B). With reference to WT livers, livers of Ch25h^{-/-} mice under an HFD were enriched in DEGs involved in pathways of positive regulation of lipid metabolic process (GO:0045834), steroid metabolic process (GO:0008202), cholesterol metabolic process (GO:0008203), and bile acid biosynthetic process (GO:0006699) (Figure 4C). A heat map showed that HFD feeding robustly reduced the hepatic levels of genes involved in steroid hormone biosynthesis, primary bile acid biosynthesis, and bile secretion in both WT and Ch25h^{-/-} mice (Figure 4D). Altogether, results in Figure 3B to 3D agree with the role of Ch25h in the immune response and the inhibitory effect of HFD on cholesterol catabolism in the liver.^{25,26} Nevertheless, the expression of genes related to steroid hormone biosynthesis, primary bile acid synthesis, and bile acid secretion (eg, CYP7A1, CYP27A1, CYP8B1, SLC27A5) was slightly higher in livers of Ch25h^{-/-} mice fed an HFD than their WT counterparts (Figure 4D), although Ch25h^{-/-} mice had more exacerbated steatosis, as seen in Figure 2A. To this end, we created a KEGG pathway of bile acid synthesis (hsa00120) (Figure 4E) for a global assessment of bile acid metabolism responding to HFD and Ch25h loss. Overall, HFD hindered the CYP7A1-regulated classical bile acid and CYP27A1-regulated alternative pathways in both WT and Ch25h^{-/-} mice. More specifically, members of the CYP7A1-regulated pathway (ie, CYP7A1, CYP8B1, and AKR1D1) were less suppressed in Ch25h^{-/-} than WT livers by an HFD (Figure 4E). This finding agreed with the highest induction of LXR in Ch25h^{-/-} mice fed an HFD (Figure 4E).

We then performed bulk assays to further interrogate the disparity between the CYP7A1 mRNA and steatosis phenotype. At a glance, HFD reduced the hepatic expression of CYP7A1 and CYP27A1 mRNA (top and bottom panels in Figure 4F) and protein (lanes 1, 2 vs lanes 5, 6; lanes 3, 4 vs lanes 7, 8 in Figure 4G). Although qPCR analysis confirmed the slightly higher mRNA level of CYP7A1 in livers of Ch25h^{-/-} than WT mice fed an HFD (lane 3 vs lane 4 in top panel of Figure 4F), Western blot analysis revealed lower level of CYP7A1 in Ch25h^{-/-} mice (lanes 5, 6 vs lanes 7, 8 in Figure 4G). To associate the expression of CYPs with bile acid production and secretion, we measured total bile acid in the liver, circulation, and feces of the 4 groups of mice. As anticipated, HFD feeding increased the bile acid content in liver, serum, and feces of both WT and Ch25h^{-/-} mice (Figure 4H). However, bile acid levels were significantly lower in liver, serum, and feces of Ch25h^{-/-} than WT mice (Figure 4H). Thus, livers of Ch25h^{-/-} mice fed an HFD, with the lowest CYP7A1 expression, would have the most severe steatosis among the 4 groups.

Ch25h Overexpression Alleviates HFD-induced Hepatic Steatosis

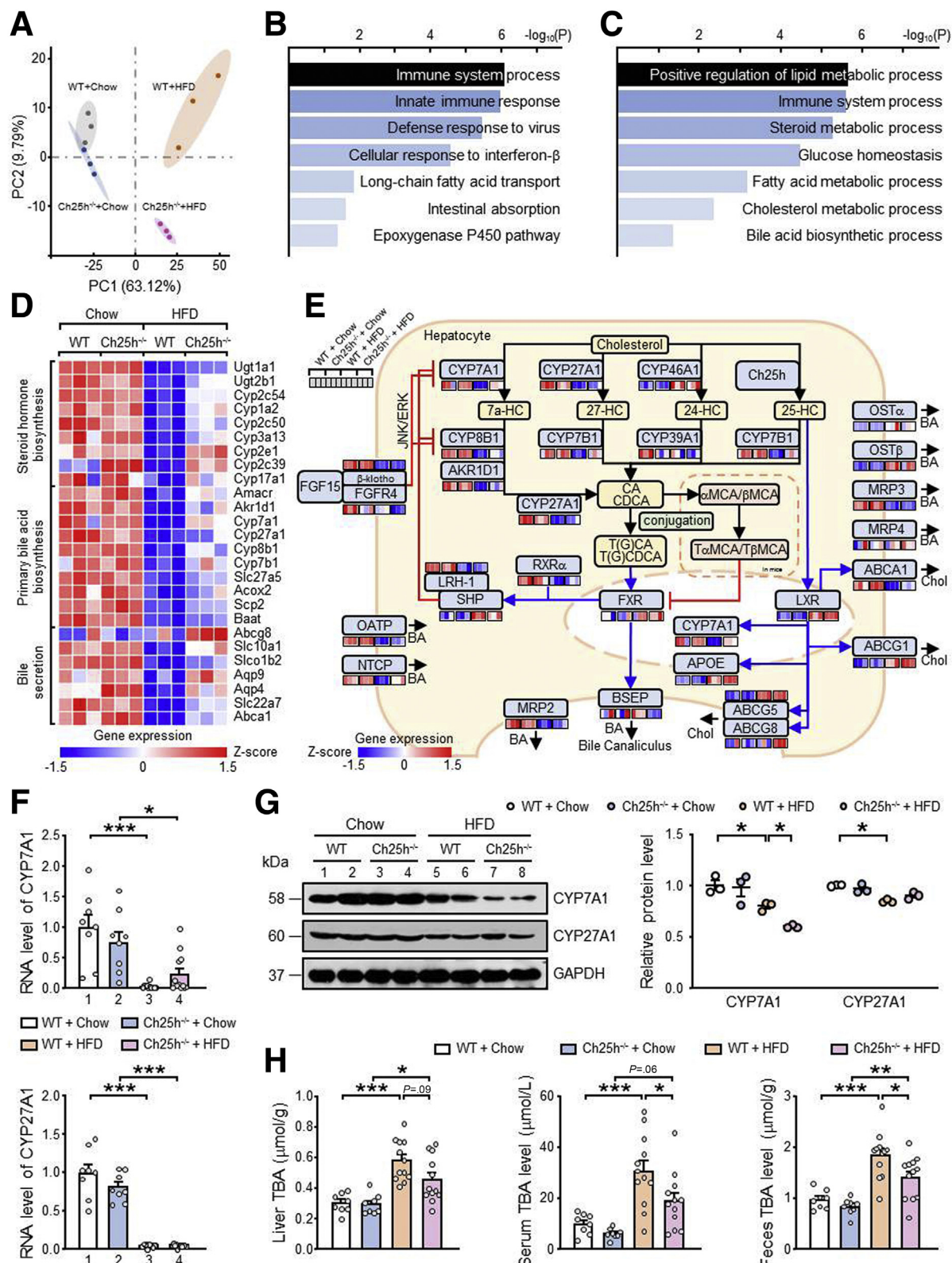
Given that Ch25h deficiency was associated with NAFLD via impaired bile acid metabolism, we next examined whether exogenously delivered Ch25h could mitigate NAFLD in mouse models. The AAV8 vector was used for hepatic overexpression of Ch25h in C57BL/6J mice. Eight-week-old male mice were administered AAV8-Ch25h or AAV8-control, then fed an HFD for 12 weeks (Figure 5A). Level of Ch25h was significantly elevated in the liver of mice receiving AAV8-Ch25h (Figure 5B). Ectopic expression of Ch25h in liver in these animals markedly alleviated the HFD-induced NAFLD, as characterized by decreased lipid accumulation and hepatic steatosis (Figure 5C, 5D), liver weight, and liver-to-body-weight ratio (Figure 5E), as well as hepatic levels of TC and TG (Figure 5F) and serum levels of TC, TG, and LDL-C (Figure 5G). For hepatic steatosis-associated inflammation, hepatic mRNA levels of interleukin 6 (IL-6), IL-1 β , tumor necrosis factor α (TNF α), and monocyte chemoattractant protein 1 (MCP-1) were significantly decreased by AAV8-Ch25h administration (Figure 5H). Additionally, compared with AAV8-control mice, the mRNA expression of lipogenic genes, such as SREBP1c, FASN, Cd36, and Elovl6, were reduced in mice injected with AAV8-Ch25h (Figure 5I). Conversely, the mRNA expression of genes involved in fatty acid β -oxidation (Acox1, Acox2, Cpt2, Acs1, Acadl, Acaa1a, and Ehhadh), and VLDL secretion (ApoB, Mttp) were all substantially increased in AAV8-Ch25h mice as compared with the AAV8-control mice (Figure 5J and 5K). In a separate set of experiments, we administered AAV8-Ch25h or AAV8-control at week 8 of HFD feeding (Figure 6A). HFD feeding lasted for another 8 weeks before mice were sacrificed. Mice receiving AAV8-Ch25h showed mitigated steatosis as compared with controls receiving AAV8-control (Figure 6A–6D), so the exogenously expressed Ch25h could reverse the onset of NAFLD in mice.

Ch25h Overexpression Increases the Synthesis and Excretion of Bile Acids

Next, we examined whether the Ch25h-mitigated steatosis in mice fed an HFD resulted from rectified bile acid metabolism in the enterohepatic system. Using data from liquid chromatography-tandem mass spectrometry, we compared constituents and levels of bile acids in liver and intestine of mice fed an HFD and administered AAV8-Ch25h or AAV8-control virus. Ch25h overexpression significantly

Figure 3. (See previous page). Ch25h deficiency aggravates HFD-induced hepatic steatosis. (A) Representative livers of WT and Ch25h^{-/-} mice fed a chow diet ($n = 8$ mice/group) or HFD for 8 weeks ($n = 12$ mice/group). (B) Liver weight. (C) Liver weight/body weight ratio. (D) Representative hematoxylin and eosin staining. Scale bars, 50 μ m. (E) Steatosis score. (F) Representative Oil-red O staining. Scale bars, 50 μ m. (G) Hepatic TC level. (H) Hepatic TG level. (I) Serum LDL-C level. (J–K) RT-qPCR analysis of mRNA levels of lipogenic genes (J), fatty acid β -oxidation genes (K), and VLDL secretion genes (L) in livers from HFD-fed WT and Ch25h^{-/-} mice ($n = 8$ mice/group). (M) VLDL-TG secretion. WT and Ch25h^{-/-} male mice (8 weeks old) were fasted for 8 hours and injected with tyloxapol (500 mg/kg in PBS) via tail veins. Blood samples were collected from the retro-orbital plexus at the indicated time point post treatment, and plasma TG levels were measured using enzymatic kits ($n = 3$ mice/group). Data are mean \pm SEM. For data in (B, C, E, G–I), significance was determined by the 1-way analysis of variance test between multiple groups. Significance of data in (J–M) was determined by the Student 2-tailed *t* test. * $P < .05$; ** $P < .01$; *** $P < .001$.

elevated total bile acid in liver (Figure 7A). Levels of both primary bile acids (CA, CDCA, UDCA, α MCA, β MCA, TCA, TCDCA, TUDCA, and T α MCA) and secondary bile acids (DCA, HDCA, ω MCA, LCA, TDCA and THDCA) were markedly increased in livers (Figure 7B and 7C). A heat map summarizing data in Figure 7B and 7C is shown in Figure 7D.



Overall, mice receiving AAV8-Ch25h increased their bile acid production, in comparison with those having AAV8-control. Consistently, total bile acid levels were significantly higher in feces of mice administered AAV8-Ch25h than AAV8-control (Figure 7E). However, bile acid metabolite in intestines of AAV8-Ch25h and AAV8-control mice were comparable (data not shown). Regarding genes regulating bile acid metabolism, Ch25h overexpression in the liver decreased CYP7A1 mRNA level (Figure 7F), but increased CYP7A1 protein (Figure 7G), which were in the opposite direction to those seen in Ch25h^{-/-} mice (Figure 4F and 4G). Also, the expression of Shp and FGFR4 was decreased by Ch25h overexpression (bottom panels of Figure 7F), which is consistent with their inhibitory effect on CYP7A1.¹⁰ Given that CDCA and DCA bind to the intestinal apical sodium-dependent bile acid transporter (ASBT) to activate the FXR/FGF15/19 pathway,¹⁰ we found that FGF15 mRNA level was significantly higher, but that of ASBT tended to be lower in the ileum of AAV8-Ch25h administered mice, when compared with control group receiving AAV8-control (Figure 7H).

25-HC Administration Mitigates HFD-induced Steatosis

Because Ch25h catalyzes the conversion of cholesterol to 25-HC, we administered 25-HC to HFD-fed mice to test the efficacy of 25-HC in intervening the HFD-induced steatosis in mice. C57BL/6J male mice were fed an HFD for 8 weeks together with daily intraperitoneal injection of 25-HC or 0.3% ethanol as a vehicle control (Figure 8A). Although body weights of 25-HC treatment and vehicle control mice had no significant difference (data not shown), 25-HC administration mitigated the HFD-induced lipid accumulation (Figure 8B), steatosis score (Figure 8C), liver/body weight ratio (Figure 8D), hepatic levels of TC and TG (Figure 8E), serum levels of TC and TG (Figure 8F), but elevated high-density lipoprotein cholesterol level (Figure 8F). Hepatic mRNA expression of genes encoding Acox1, Cpt2, Acsl1, Acadl, Acaa1a, ApoB, and Mttp were higher in the 25-HC treatment mice than in the vehicle-treated control mice (Figure 8G and 8H). The protein level of ApoB100/48 in the isolated plasma VLDL fraction was also remarkably increased in 25-HC administered mice (Figure 8I). Hepatic mRNA levels of inflammatory genes,

such as IL-6, IL-1 β , TNF α , and MCP-1, were lower in the 25-HC treatment mice than in the vehicle-treated control mice (Figure 8J). These beneficial effects of 25-HC would be due in part to the improved enterohepatic circulation of cholesterol/bile acids, as evidenced by the elevation of hepatic level of CYP7A1 (Figure 8K).

Discussion

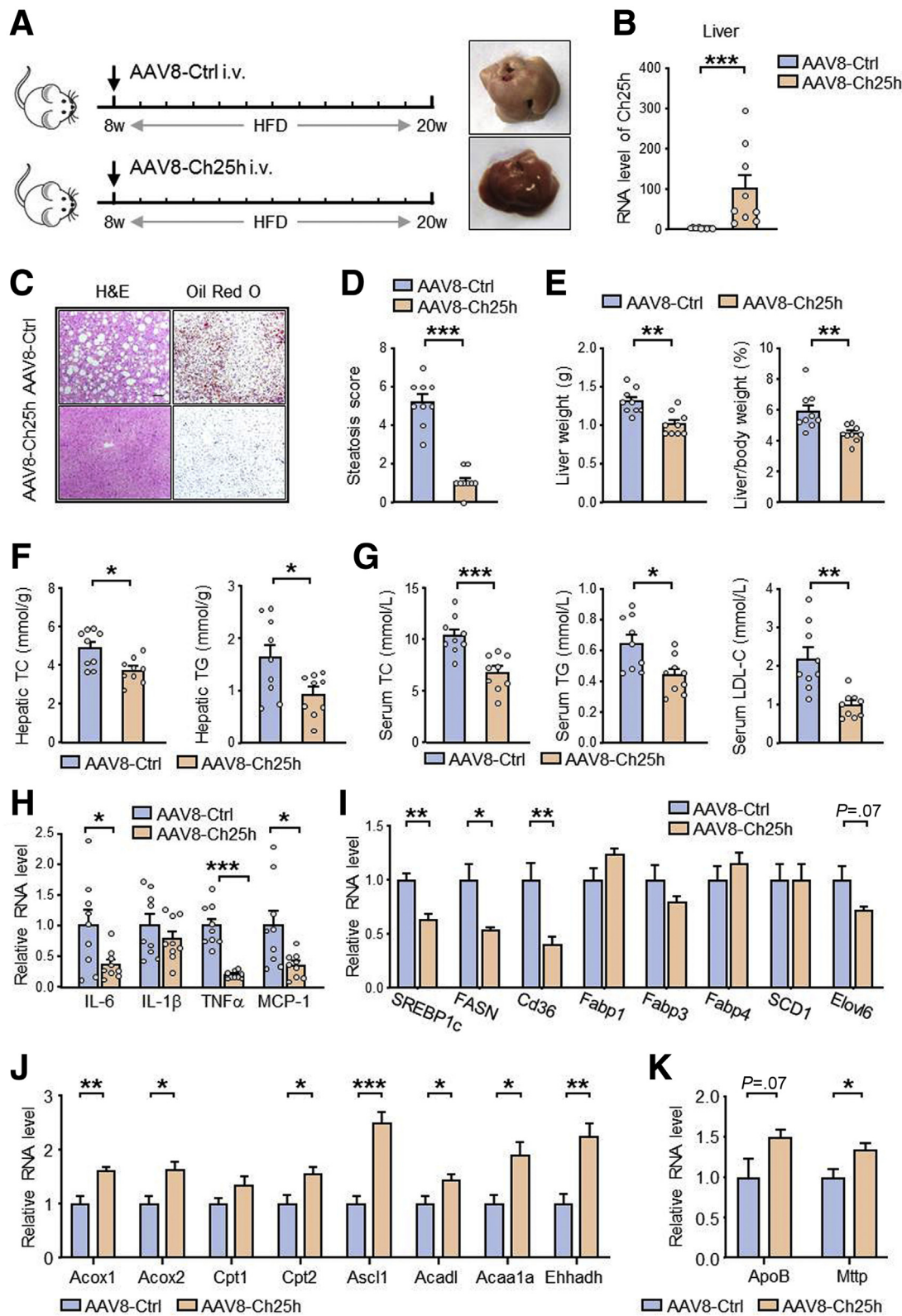
The key finding of this study is that elevated levels of Ch25h and its enzymatic product 25-HC in liver protect against HFD-induced hepatic steatosis by regulating enterohepatic circulation of cholesterol and bile acids. This conclusion was based on mouse models with gain- and loss-of-function of Ch25h or fed 25-HC. In rodent hepatocytes, LXR α transactivates CYP7A1.^{7,27} Given that 25-HC feeding increased CYP7A1, the underlying mechanism would be 25-HC activation of CYP7A1 via LXR α . As a result, hepatic biosynthesis of bile acids is enhanced, which acts against the HFD-induced steatosis (seen in graphical abstract).

Ch25h is a member of the family of lipid desaturases and hydroxylases and an important regulator of cholesterol homeostasis by activating LXR while inhibiting SREBP2.^{16,17} Previous studies demonstrated that LXR α ablation in mice impairs the conversion of cholesterol to bile acids and confers a fatty liver phenotype.²⁷ In this study, we provide several lines of evidence demonstrating that Ch25h activates LXR α and its target CYP7A1 via 25-HC in the context of liver steatosis in mouse. First, Ch25h^{-/-} mice phenotypically copied LXR α ^{-/-} mice (Figure 3), which suggests the causal effect between Ch25h and LXR in regulating cholesterol/bile acid metabolism in the rodent liver. This causality relies on the presence of an LXR response element in the promoter region of the rodent CYP7A1 gene.²⁸ Such thesis is supported by the observation that LXR α target gene CYP7A1 were upregulated in mouse primary hepatocytes with Ch25h overexpression, which was abolished by the LXR α antagonist (Figure 2D). Furthermore, CYP7A1 were downregulated in hepatocytes isolated from Ch25h^{-/-} mice (Figure 2C). These complimentary changes suggest the hierarchical role of the Ch25h-LXR α -CYP7A1 axis in regulating bile acid metabolism in mouse models. Due to the lack of LXR putative binding site in the promoter region of the human CYP7A1 gene,²⁹ we wondered whether Ch25h has an inducing effect on CYP7A1 expression in human

Figure 4. (See previous page). Ch25h deficiency alters bile acid metabolism and the expression of bile acid-related genes. (A-E), Ch25h^{-/-} mice and their Ch25h^{+/+} (WT) littermates were fed a chow diet or HFD for 8 weeks. Total RNA was extracted from liver tissues then underwent RNA-sequencing analysis ($n = 3$ mice/group). (A) Two-way principal component analysis (PCA) plot. Percentages indicate the proportion of variance explained by each component. (B, C) GO enrichment analysis with use of the Database for Annotation, Visualization, and Integrated Discovery (DAVID) of differentially expressed genes and plotted as $-\log(P$ value). (B) Shows WT + chow diet vs Ch25h^{-/-} + chow diet, whereas (C) shows WT + HFD vs Ch25h^{-/-} + HFD. (D) Heat map comparison of the 4 groups (WT or Ch25h^{-/-} under chow or HFD) using FPKM of the indicated genes. (E) KEGG pathway of bile acid synthesis (hsa00120). (F) qPCR analysis of mRNA levels of CYP7A1 and CYP27A1 in livers of WT and Ch25h^{-/-} mice fed a chow diet or HFD for 8 weeks. (G) Western blot analysis of CYP7A1 and CYP27A1 in livers of WT and Ch25h^{-/-} mice fed an HFD for 8 weeks. GAPDH was used as a loading control. (H) Total bile acid levels in liver, serum, and feces from WT and Ch25h^{-/-} mice fed an HFD for 8 weeks ($n = 8-12$ mice/group). Data are mean \pm standard error of the mean. For the upper panel in (F), significance was determined by Kruskal-Wallis with Dunn post hoc test. For data in (G, H) and the lower panel in (F), significance was determined by the 1-way analysis of variance test between multiple groups. * $P < .05$; ** $P < .01$; *** $P < .001$.

hepatocytes. To test so, we knocked down Ch25h in HepG2 cells. Resulting from Ch25h knockdown, the mRNA and protein levels of LXR α , CYP7A1, and CYP27A1 were all decreased (Figure 9A and 9B). In contrast, Ch25h

overexpression in HepG2 cells increased the mRNA and protein levels of LXR α , CYP7A1, and CYP27A1 (Figure 9C and 9D). This opposite effect between Ch25h knockdown and overexpression on CYP7A1 expression in HepG2 cells



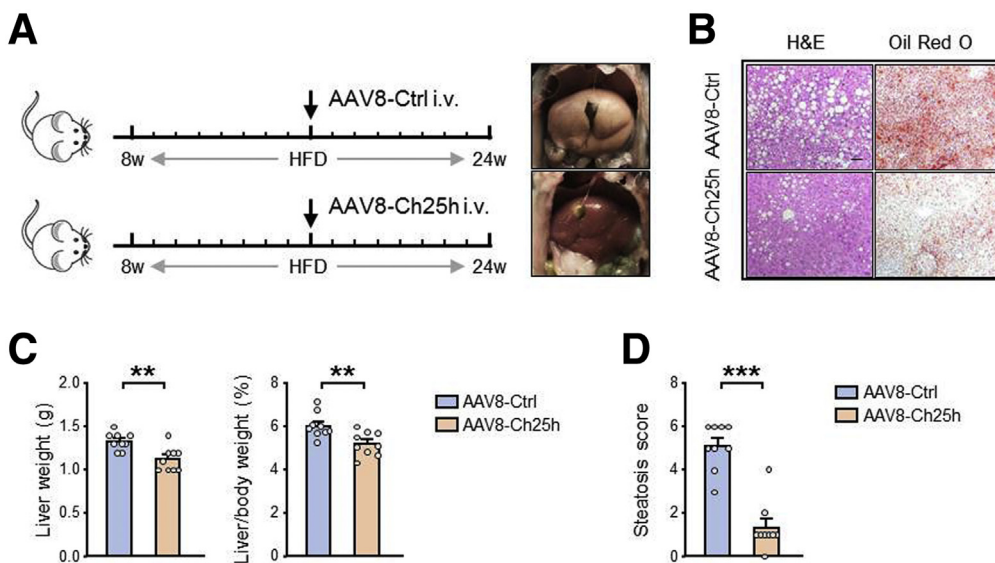


Figure 6. Exogenously expressed Ch25h reverses HFD-induced hepatic steatosis. (A) Representative liver images of C57BL/6J mice fed an HFD for 16 weeks, and at the eighth week, AAV8-Ch25h or AAV8-control was administered ($n = 9$ mice/group). (B) Hematoxylin and eosin (H&E) and Oil-red O staining. Scale bars, $50 \mu\text{m}$. (C) Liver weight and liver weight/body weight ratio. (D) Steatosis score. Data are mean \pm standard error of the mean. For left panels in (C) and data in (D), significance was determined by the Mann-Whitney *U* test. For right panels in (C), significance was determined by the Student 2-tailed *t* test. ** $P < .01$; *** $P < .001$. i.v., Intravenous.

implies that Ch25h production of 25-HC may be beneficial in human hepatocytes as well. However, the upregulation of CYP7A1 by Ch25h in human hepatocyte, if it is, would be independent of LXR α . Given LXR activation is both beneficial and deleterious for various metabolic processes, Ch25h and 25-HC induction of bile acid production via LXR-independent mechanism may provide new therapeutic strategy for NAFLD.

Bile acids can be synthesized via the CYP7A1-regulated classic bile acid pathway and CYP27A1-regulated alternative pathway.¹⁰ We found the hepatic mRNA and protein levels of CYP27A1 neither significantly increased nor decreased in Ch25h gain- and loss-of-function mouse models (Figure 7F and 7G and Figure 4F and 4G). This result supports that the classic bile acid pathway (predominantly regulated by CYP7A1) accounts for the bile acid biosynthesis in response to Ch25h.

Cholesterol conversion to bile acids is activated by LXR, but bile acid synthesis is inhibited by FXR via its suppression of CYP7A1.^{6,30} Mice receiving AAV8-Ch25h showed

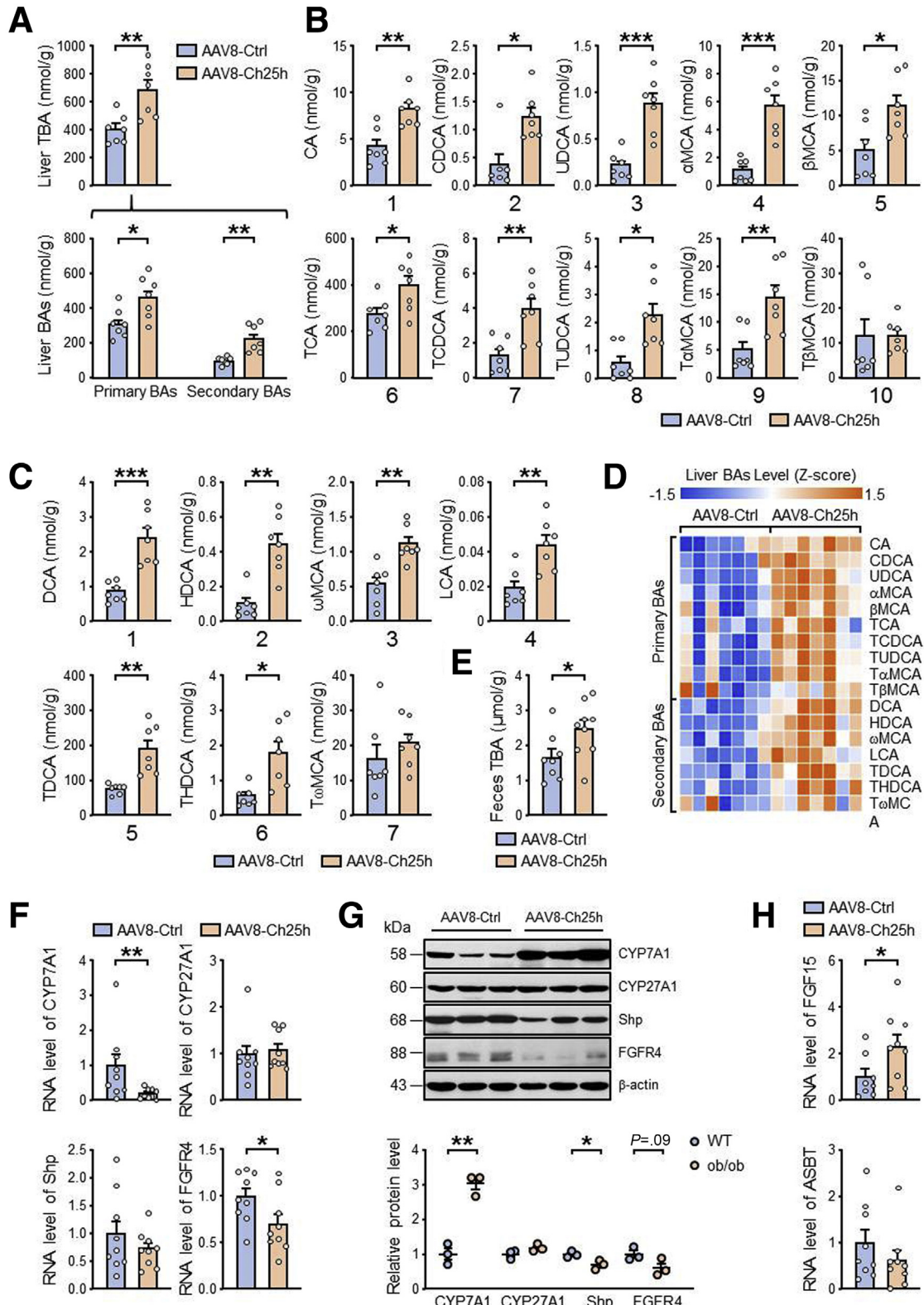
increased proportion of bile acids that are ligands of FXR (ie, CA, CDCA, LCA, DCA) in the liver and elevated FGF15 level in the ileum. These changes should provide a negative feedback by the FXR-FGF15-FGFR4 pathway to inhibit CYP7A1 transcription. Intriguingly, the mRNA and protein levels of CYP7A1 were in the opposite direction in both Ch25h gain- and loss-of-function mice *in vivo* and isolated hepatocytes (Figure 7F and 7G; Figure 4F and 4G; Figure 2A and 2C). These discrepancies may be due to an acute feedback suppression of Ch25h transcription by FXR-FGF15-FGFR4 but a longer life of CYP7A1 protein in the mouse liver. To test this possibility, we administered AAV8-Ch25h to C57BL/6J mice and livers were harvested 3 days post-virus administration. The mRNA level of CYP7A1 had already decreased, but the protein level was increased (Figure 10).

Levels of primary bile acids (eg, CA, CDCA) and also secondary bile acids (eg, DCA, LCA) were increased in mouse livers with Ch25h overexpression (Figure 7A–7D). Therefore, besides CYP7A1, intestinal bacterial flora is involved in the increased bile acid biosynthesis regulated by

Figure 5. (See previous page). Ch25h overexpression alleviates HFD-induced fatty liver. (A) Representative liver images of C57BL/6J mice administered AAV8-control or AAV8-Ch25h, then fed an HFD for 12 weeks ($n = 9$ mice/group). (B) RT-qPCR analysis of hepatic Ch25h mRNA level. (C) Hematoxylin and eosin (H&E) and Oil-red O staining. Scale bars, $50 \mu\text{m}$. (D) Steatosis score. (E) Liver weight and liver weight/body weight ratio. (F) Hepatic TC and TG levels. (G) Serum TC, TG, and LDL-C levels. (H) Hepatic expression of mRNAs encoded by inflammatory-related genes (IL-6, IL-1 β , TNF α , and MCP-1) from AAV8-control or AAV8-Ch25h-injected mice fed an HFD for 12 weeks ($n = 9$ mice/group). (I–K) Hepatic expression of mRNAs encoded by lipogenesis-related genes (SREBP1c, FASN, Cd36, Fabp1, Fabp3, Fabp4, SCD1, and Elovl6) (I), fatty acid β -oxidation related genes (Acox1, Acox2, Cpt1, Cpt2, Ascl1, Acadl, Acaa1a, and Ehhadh) (J), and VLDL secretion-related genes (ApoB and Mtpp) (K) from AAV8-control and AAV8-Ch25h injected mice fed an HFD for 8 weeks ($n = 8$ –9 mice/group). Data are mean \pm standard error of the mean. For data in (D) and left panels in (E, F), significance was determined by the Mann-Whitney *U* test. For right panels in (E, F), and data in (G–K), significance was determined by the Student 2-tailed *t* test. * $P < .05$, ** $P < .01$; *** $P < .001$. i.v., Intravenous.

hepatic activation of the Ch25h–25-HC axis. Several studies reported that microbiota convert primary to secondary bile acids in the ileum via deconjugation and 7 α -

dehydroxylation.^{31,32} Jiang et al showed that antibiotics treatment in mice increased the level of conjugated bile acids, which inhibited intestinal FXR signaling.³³ Kim et al



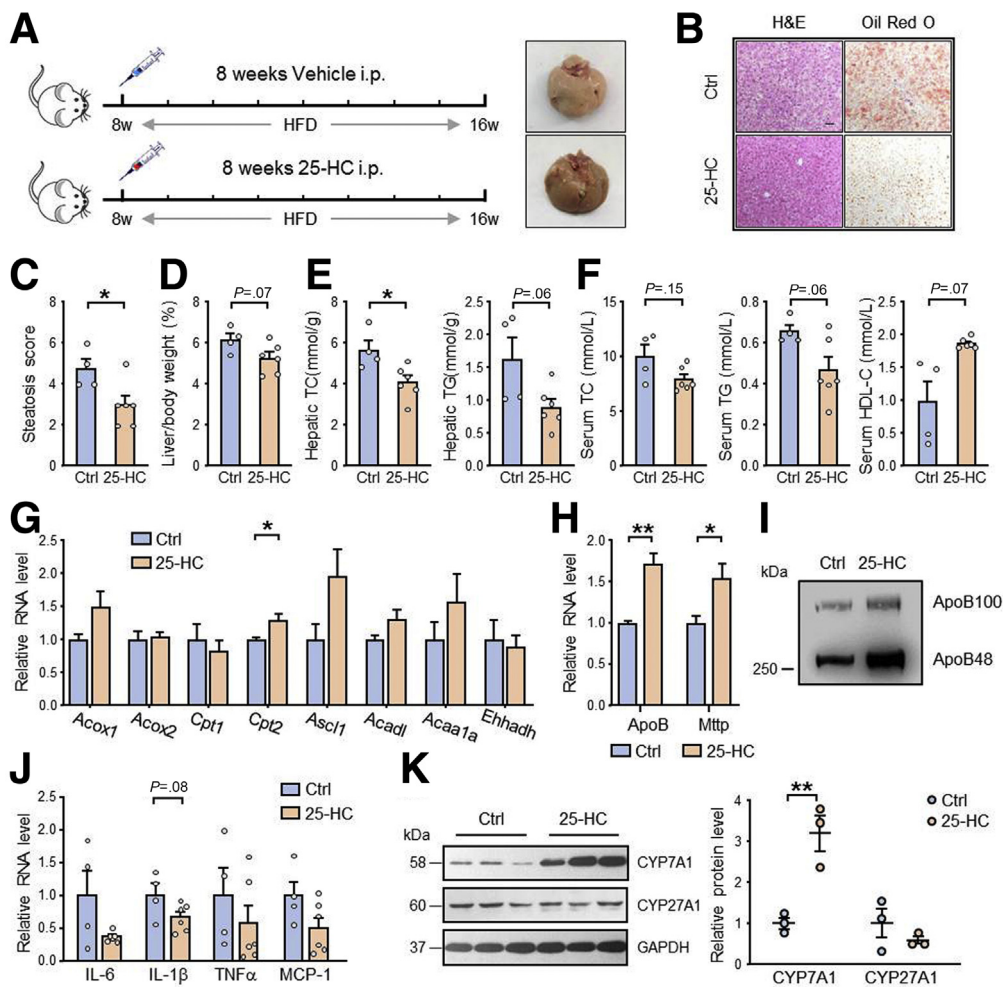


Figure 8. Administration of 25-HC improves HFD-induced hepatic steatosis. (A, B) Representative liver photographs (A) and hematoxylin and eosin (H&E) and Oil-red O staining (B) of C57BL/6J mice fed an HFD for 8 weeks together with daily intraperitoneal (i.p.) injection of 25-HC ($n = 6$) or 0.3% ethanol as a vehicle control ($n = 4$). Scale bars, 50 μ m. (C) Steatosis score. (D) Liver weight/body weight ratio. (E) Hepatic TC and TG levels. (F) Serum TC, TG, and high-density lipoprotein-cholesterol (HDL-C) levels. (G, H) Hepatic mRNA levels of fatty acid β -oxidation genes (G), and VLDL secretion genes (H) from vehicle or 25-HC injected mice fed an HFD for 8 weeks ($n = 4\text{--}5$ mice/group). (I) Western blot analysis of ApoB protein level in plasma VLDL fraction. The aliquots of pooled plasma from 3 mice in each group were used for VLDL isolation. The plasma VLDL was fractionated by density gradient centrifugation ($d \leq 1.006$). (J) Hepatic mRNA levels of inflammatory-related genes (IL-6, IL-1 β , TNF α , and MCP-1) from vehicle or 25-HC-injected mice fed an HFD for 8 weeks ($n = 4\text{--}6$ mice/group). (K) Western blot analysis of CYP7A1 and CYP27A1 in livers from vehicle or 25-HC-injected mice fed an HFD for 8 weeks ($n = 3$ mice/group). Data are mean \pm standard error of the mean. For (C, D, F-H, J, K) and left panel in (E), significance was determined by the Student 2-tailed t test. For the right panel in (E), significance was determined by the Mann-Whitney U test. * $P < .05$; ** $P < .01$.

Figure 7. (See previous page). Ch25h overexpression increases the synthesis and excretion of bile acids (BAs). (A) Content of total BA (TBAs) and primary and secondary BAs in livers of AAV8-control and AAV8-Ch25h-injected mice fed an HFD for 8 weeks ($n = 7$ mice/group). (B) Primary BA levels. (C) Secondary BA levels. (D) Heat map summary of primary and secondary BAs in livers of AAV8-control and AAV8-Ch25h-administered mice fed an HFD for 8 weeks ($n = 7$ mice/group). (E) Total BA levels in feces of AAV8-control ($n = 8$) and AAV8-Ch25h-injected mice ($n = 9$) fed an HFD for 8 weeks. (F) mRNA levels of BA-related genes (CYP7A1, CYP27A1, Shp, and FGFR4) in livers from AAV8-control or AAV8-Ch25h-injected mice fed an HFD for 8 weeks ($n = 9$ mice/group). (G) Western blot analysis of protein levels of CYP7A1, CYP27A1, Shp, and FGFR4 in livers from AAV8-control and AAV8-Ch25h-injected mice fed an HFD for 8 weeks ($n = 3$ mice/group). (H) Intestine mRNA levels of FGF15 (upper panel) and ASBT (lower panel) from AAV8-control ($n = 8$) or AAV8-Ch25h-administered mice ($n = 9$) fed an HFD for 8 weeks. Data are mean \pm standard error of the mean. For data in (A, E, and G), panel 1, and 3-7 in (B) and (C), lower panels in (F), and upper panels in (H), significance was determined by the Student 2-tailed t test. For panel 2, and 8-10 in (B), panel 2 in (C), the upper panels in (F), and the lower panel in (H), significance was determined by the Mann-Whitney U test. * $P < .05$; ** $P < .01$; *** $P < .001$.

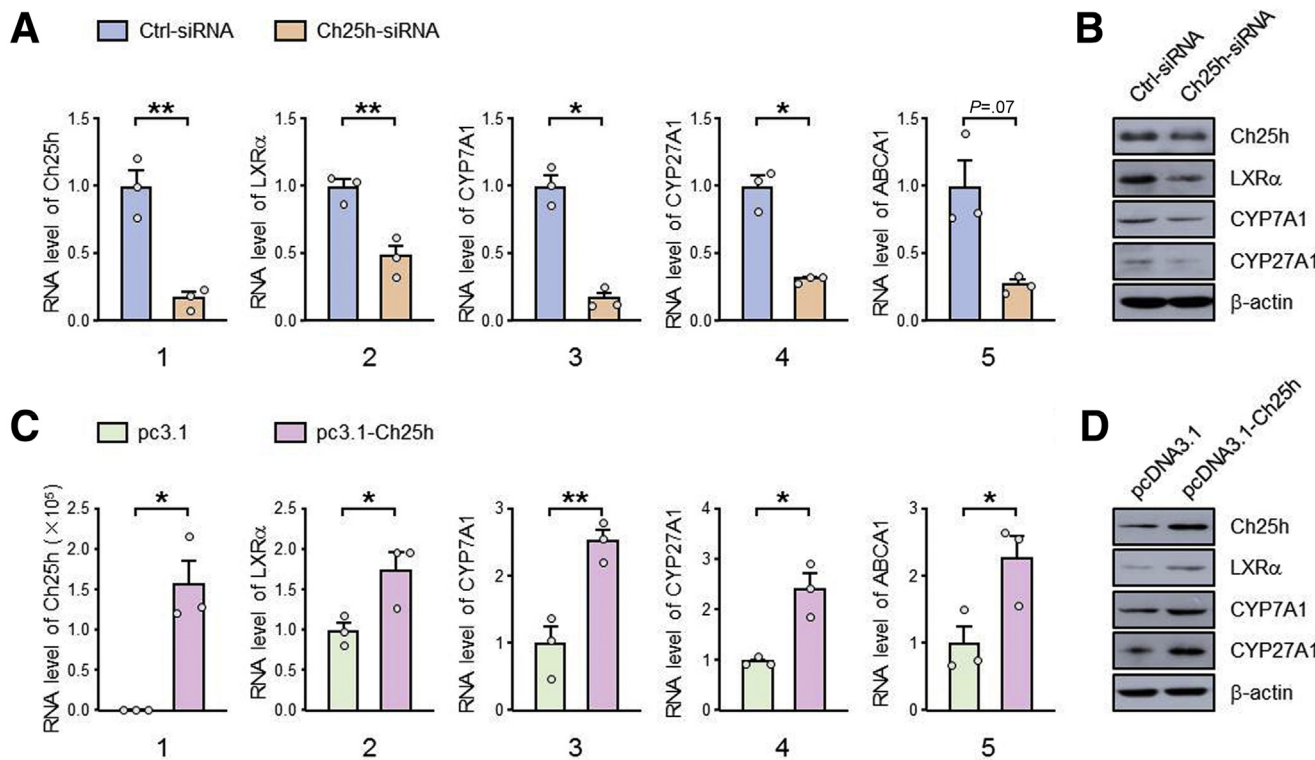


Figure 9. Ch25h positively regulates CYP7A1 and CYP27A1 in cultured HepG2 cells. (A) RT-qPCR analysis of mRNA levels of Ch25h, LXR α , CYP7A1, CYP27A1, and ABCA1 in HepG2 cells transfected with Ctrl-siRNA or Ch25h-siRNA. (B) Western blot analysis of protein levels of Ch25h, LXR α , CYP7A1, CYP27A1, and ABCA1 in HepG2 cells transfected with Ctrl-siRNA or Ch25h-siRNA. (C) qPCR analysis of mRNA levels of Ch25h, LXR α , CYP7A1, CYP27A1, and ABCA1 in HepG2 cells transfected with pcDNA3.1 or pcDNA3.1-Ch25h. (D) Western blot analysis of Ch25h, LXR α , CYP7A1, and CYP27A1 in HepG2 cells transfected with pcDNA3.1 or pcDNA3.1-Ch25h. Data are presented as mean \pm standard error of the mean. For panels 1, 2, 4, 5 in (A) and panels 1, 3–5 in (C), significance was determined by the Student 2-tailed *t* test. For panel 3 in (A) and panel 2 in (C), significance was determined by the Mann-Whitney *U* test. **P* < .05; ***P* < .01.

demonstrated that FXR activation in the intestine is required for short-term CYP7A1 repression in liver.³⁰ In agreement with these results, we found that Ch25h overexpression in liver might activate intestinal FXR signaling

via FGF15 induction (Figure 7H), which would suppress the transcription of CYP7A1.

Emerging evidence showed that Ch25h also acts as an immune regulator via its regulation of innate immunity and

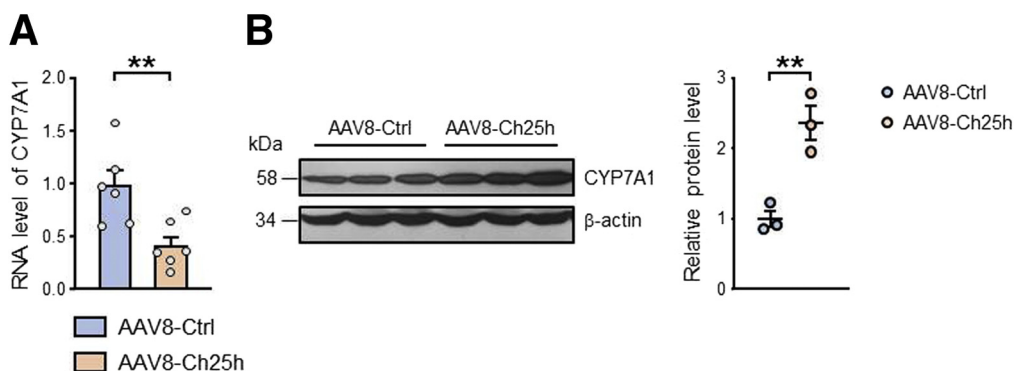


Figure 10. Ch25h overexpression regulates CYP7A1 expression. (A) RT-qPCR analysis of mRNA levels of CYP7A1 in livers of AAV8-control and AAV8-Ch25h-injected mice fed a chow diet for 3 days (*n* = 6 mice/group). (B) Western blot analysis of CYP7A1 protein level in livers of AAV8-control and AAV8-Ch25h-injected mice fed a chow diet for 3 days (*n* = 3 mice/group). Data are mean \pm standard error of the mean. Significance for data in (A) and (B) was determined by the Student 2-tailed *t* test. ***P* < .01.

antiviral effect.¹⁸ Ch25h deficiency leads to IL-1 production with ensuing inflammatory insults.²⁶ In contrast, 25-HC represses NLRP3 inflammasome in macrophages.¹⁸ Our previous study showed that Ch25h-25-HC activation in vascular endothelium and monocytes/macrophages is athero-protective via its anti-inflammatory effect.³⁴ Although a 12-week period of HFD feeding could not result in obvious inflammatory cell infiltration, the levels of inflammatory genes, such as IL-6, IL-1 β , TNF α , and MCP-1 were significantly lower in livers of AAV-Ch25h or 25-HC treated mice than in controls (Figure 5H and Figure 8J). As such, the reduced hepatic inflammation by Ch25h overexpression or 25-HC administration would result, in part, from their inhibition of the SREBP-induced innate immune response.

Therapeutic options for NAFLD are lacking. The efficacy of several agents, such as agonists of FXR (ie, obeticholic acid), PPAR α , and PPAR δ agonist (ie, elafibronor, thiazolidinedione) and antagonist against CCR2 and CCR5 (ie, cencriviroc), has been tested in clinical trials.^{2,35-37} Although these agents alleviate steatosis, unwanted effects are evident in some individuals.^{2,38} Because of the significant effect of Ch25h overexpression and exogenously administered 25-HC in ameliorating hepatic steatosis and expression of inflammatory genes as we showed herein, drugs and compounds that result in activation of the Ch25h-25-HC axis might have therapeutic potential for NAFLD. The underlying mechanism may involve bile acid production and secretion, which is supported by the immensely increased bile acid levels found in livers and feces from the Ch25h-25-HC gain-of-function mice. This beneficial effect is reminiscent of using non-systemically absorbed resins in treating NAFLD in humans. Targeting Ch25h or 25-HC might have additional therapeutic advantages, given that 25-HC is an endogenous cholesterol-derivative.

In summary, our results show that during the onset of NAFLD in mice under an HFD, Ch25h suppression in the liver blunted the CYP7A1-dependent bile-acid biosynthesis and secretion, which worsened hepatic steatosis. In contrast, activation of the Ch25h-25-HC axis resulted in massive production and secretion of bile acids, which facilitated the hepatic cholesterol homeostasis. Of note, activation of this axis in mouse liver also changed lipid metabolism, such as inhibition of lipogenesis, promotion of fatty acid oxidation and VLDL secretion, and improved glucose tolerance and insulin sensitivity.²² Thus, activation of the Ch25h-25-HC pathway may be beneficial in restoring metabolic homeostasis in general.

Methods

Animal Experiments

All animal protocols were approved by the Institutional Animal Care and Use Committee of Xi'an Jiaotong University (approval no. XJTULAC2017.581). The animals received humane care according to the criteria outlined in the Guide for the Care and Use of Laboratory Animals prepared by the National Academy of Sciences and published by the National Institutes of Health. ob/ob mice were kindly provided by

Laboratory Animal Resources Center, Tsinghua University. E3 rats were originated from the Section of Medical Inflammation Research, Lund University, Sweden.²³ Liver samples were obtained from ob/ob mice aged 6 months and with severe hepatic steatosis. Control livers were collected from C57BL/6J mice at a corresponding age. Liver samples were also collected from E3 rats fed an HFD (36% of total energy as fat) for 12 weeks. Control samples were collected from E3 rats fed a chow diet. Global Ch25h-knockout mice (Ch25h $^{-/-}$) were purchased from The Jackson Laboratory and genotyped as described.³⁴ The corresponding Ch25h $^{+/+}$ (WT) littermate control mice were obtained from cross-breeding Ch25h $^{+/+}$ mice. Male mice used in this study were housed under a 12-hour light/dark cycle, in a pathogen-free animal facility at Xi'an Jiaotong University. Mice were maintained on a standard rodent chow or an HFD (D12109C, Research Diets) for 8 weeks and water ad libitum.

Three mouse models were used in this study. In the first model, C57BL/6J male mice aged 8 weeks were injected with AAV8-GFP (AAV8-control) or AAV8-Ch25h vectors via the tail vein (2×10^{11} vg/mouse), then fed an HFD for 12 weeks. In the second model, C57BL/6J mice were fed an HFD for 16 weeks and at the eighth week, were injected with AAV8-Ch25h or AAV8-control via the tail vein (2×10^{11} vg/mouse). In the third model, C57BL/6J male mice (8-week-old) fed an HFD for 8 weeks together with daily intraperitoneal injection of 25-HC (50 mg/kg) or 0.3% ethanol as a vehicle control.

Histology Analysis

Liver samples were fixed in 10% formaldehyde for 24 hours, and then processed for embedding in paraffin. Sections (4- μ m thick) were cut and stained with hematoxylin and eosin. Frozen sections of liver (5- μ m thick) were stained with 0.5% Oil-red O for visualizing hepatic fat, then counterstained with hematoxylin. Histology and image processing were carried out using a Leica DMRE microscope equipped with Spot digital image analysis software and a camera.

Hepatic and Plasma Lipid Measurements

Liver samples were homogenized for extraction of lipids by the chloroform/methanol method. Hepatic TC and TG levels were determined by using the manufacturer's manuals (Nanjing Jiancheng Biotechnological Co). Blood was obtained from retro-orbital veins and serum was used for TC, TG, LDL-C, and high-density lipoprotein cholesterol determinations as above.

VLDL-TG Secretion

VLDL secretion in WT and Ch25h $^{-/-}$ mice (8 weeks old) was measured according to method previously described.³⁹ Briefly, the mice were fasted for 8 hours and then injected with Tyloxapol (Triton WR-1339, 500 mg/kg in PBS) (Sigma) via tail veins. Fifty μ l of blood were collected from the retro-orbital plexus in heparinized tubes at the indicate time points and measured for plasma TG.

Isolation of Plasma VLDL Fraction

Plasma VLDL fraction was isolated as previously described.³⁹ Briefly, the aliquots of pooled plasma from 3 mice in each group were used for VLDL isolation. One hundred μ L plasma were diluted 1:30 with 2.9 mL PBS. Next, 1.2 mL iodixanol was added to 2.75 mL mixture to obtain 15% concentration of iodixanol (D1556, Sigma). The final mixture was subjected to ultracentrifugation at 100,000 g for 90 minutes at room temperature in Optima L-100 XP Ultracentrifuge (Beckman, TYPE 100ti rotor). VLDL fraction was found on the top fraction with density less than 1.006.

Bile Acid Analyses

Liver and fecal samples were extracted with 50:50 methanol/H₂O and 5% ammonium hydroxide in acetonitrile. Total bile acids were measured by using the manufacturer's manuals (Nanjing Jiancheng Biotechnological Co.). Quantification of specific bile acids in liver and ileum involved a Waters Acquity H-Class UPLC system with a Waters Acquity BEH C18 column (2.1 \times 100 mm) coupled to a Waters Xevo TQ-S.

Isolation and Culture of Primary Hepatocyte

Mouse primary hepatocytes were collected from 8 week-old WT mice and Ch25h^{-/-} mice according to the method previously described.⁴⁰ For overexpression of Ch25h, WT mice were injected with AAV8-GFP or AAV8-Ch25h via the tail vein (2×10^{11} vg/mouse) for 3 days. Cells were plated for 4 hours to permit adhesion in Dulbecco's Modified Eagle's Medium containing 10% fetal bovine serum. The cultures were then washed to remove dead or unattached cells. Thereafter, primary hepatocytes were treated with LXR antagonist (GSK2033, SML1617, Sigma-Aldrich) for 24 hours.

Cell Lines and Treatments

HepG2 cells were cultured in Dulbecco's Modified Eagle's Medium containing 10% fetal bovine serum, 100 units/ml penicillin, and 100 units/ml streptomycin at 5% CO₂ and 37 °C. siRNA for human Ch25h (5'-CCUCCACGUUGGUCAA CAUTT-3', 5'-AUGUUGACCACGUGGAAGGTT-3') and scrambled siRNA (5'-UUCUCCGAACGUGUCACGUTT-3', 5'-ACGUGACACGUUCGGAGAATT-3') were designed and synthesized by GenePharma. pcDNA3.1-Ch25h was constructed by WZ Biosciences Inc (Jinan, China). For Ch25h knockdown, HepG2 cells were deprived of serum overnight and transfected with control siRNA or Ch25h siRNA for 24 hours. For Ch25h overexpression, HepG2 cells were transfected pcDNA3.1-Ch25h for 24 hours.

RNA-sequencing (RNA-Seq)

Total RNA was extracted from liver tissues. RNA integrity was assessed by using an RNA Nano 6000 Assay Kit and an Agilent Bioanalyzer 2100 system (Agilent Technologies). The mRNA was purified from total RNA by using poly-T oligo-attached magnetic beads. RNA libraries were

generated by using a NEBNext Ultra RNA Library Prep Kit (NEB) following the Illumina manufacturer's recommendations. Library quality was assessed on an Agilent Bioanalyzer 2100 system. Clustering of the index-coded samples was performed by using a cBot Cluster Generation System with a TruSeq PE Cluster Kit v4-cBot-HS (Illumina) according to the manufacturer's instructions. Libraries were then sequenced on an Illumina NovaSeq 6000 platform (Illumina).

Functional Enrichment Analysis

The gene counts obtained from RNA-Seq were screened by using the R package DESeq2 to screen DEGs between WT and Ch25h^{-/-} mice under an HFD or chow diet ($P < .05$; logFC > 0.5) for further pathway analysis. The Morpheus online tool was used to plot a heat map (<https://software.broadinstitute.org/morpheus/>). The Database for Annotation, Visualization, and Integrated Discovery (DAVID) v6.8^(41,42) was used for GO biological process analysis of DEGs. KEGG pathway database (<https://www.genome.jp/kegg/pathway.html>) was used as reference for the pathway map.

qPCR and Immunoblotting

Total RNA was extracted from mouse and rat livers or HepG2 cells by using TRIzol reagent (Invitrogen). Reverse transcription was conducted with 1 μ g total RNA with HiScript QRT SuperMix (Vazyme). qPCR was carried out in triplicate for the amplification of specific genes and normalized by comparison with β -actin. Each PCR reaction consisting of forward and reverse primers and SYBR Green PCR Master Mix was performed by using an ABI 7500 system (Applied Biosystems). The generation of specific PCR products was confirmed by melting curve analysis, and relative gene expression changes were measured by the comparative Ct method, $X = 2^{-\Delta\Delta Ct}$. qPCR primers are shown in Table 1. For immunoblotting, liver or HepG2 cell proteins were extracted by using the RIPA kit (Beyotime). Protein samples 50 μ g were subjected to 10% SDS-PAGE, transferred to PVDF membrane, and immunoblotted by using the antibodies for Ch25h (sc-293256, Santa Cruz Biotechnology), LXR α (sc-271064, Santa Cruz Biotechnology), (CYP7A1 (ab79847, Abcam), CYP27A1 (ab126785, Abcam), Shp (ab32559, Abcam), and FGFR4 (ab178396, Abcam). Antibodies for β -actin (sc-47778, Santa Cruz Biotechnology), GAPDH (#2118S, CST), or α -tubulin (AF7010, AFFINITY) were loading controls. Detection of apoB100/48 (MA535458, Thermo Fisher) by Western blot was carried out in VLDL fractions isolated from aliquots of pooled plasma (n = 3 mice/group). Fifteen μ L of VLDL fraction were subjected to Western blot for ApoB protein expression. The protein bands were visualized by enhanced chemiluminescence (ECL; Millipore).

Statistical Analysis

All statistical analyses were performed using SPSS version 26.0. Initially, the data sets were analyzed for normality using the Shapiro-Wilk test ($P > .05$) and equal

Table 1. Primers Used for RT-qPCR

Name	Species	Sequence
Ch25h	<i>Mus musculus</i>	Forward: TTAACATCTGGCTGTCGGTG Reverse: AGAGTGCCAGCATTTGTC
LXR α	<i>Mus musculus</i>	Forward: TCTGGAGACATCTGGAGGTA Reverse: GGCCCTGGAGAACTCGAAG
CYP7A1	<i>Mus musculus</i>	Forward: AACTGGAGCTTGTAGAGAGC Reverse: CGTTACATCATCCAGTGTCC
CYP27A1	<i>Mus musculus</i>	Forward: GATCCTACATCCATTGGCT Reverse: CTCATACTTCTGTACCAGCC
SREBP1	<i>Mus musculus</i>	Forward: GCAGCCACCATCTAGCTG Reverse: CAGCAGTGAAGTCTGCCTTGAT
SREBP2	<i>Mus musculus</i>	Forward: GCTGTGAGGATGAAGGCAAG Reverse: GCTGGACCGTGGATTAC
IL-6	<i>Mus musculus</i>	Forward: CGGCCTTCCCTACTTCACAA Reverse: TTCTGCAAGTGCATCATCGT
IL-1 β	<i>Mus musculus</i>	Forward: ATGAGAGCATCCAGCTTCAA Reverse: TGAAGGAAAAGAAGGTGCTC
TNF α	<i>Mus musculus</i>	Forward: TGAGCACAGAAAGCATGATCC Reverse: GCCATTGGAACTTCTCATC
MCP-1	<i>Mus musculus</i>	Forward: AGATGCAGTTAACGCCCCAC Reverse: CCCATTCTTCTTGGGGTCA
Shp	<i>Mus musculus</i>	Forward: TCTGCAGGTGCGTCCGACTATT Reverse: AGGCAGTGCTGTGAGATGC
FGFR4	<i>Mus musculus</i>	Forward: TTGGCCCTGTTGAGCATCTT Reverse: GCCCTCTTGTACCAGTGACG
FGF15	<i>Mus musculus</i>	Forward: GCCATCAAGGACGTCA Reverse: CTTCTCCGAGTAGCGAACATG
ASBT	<i>Mus musculus</i>	Forward: TGATTTTCTATGGGTGCAAT Reverse: TGAGAGGCATGATTCAAACATG
FASN	<i>Mus musculus</i>	Forward: GGCCCCCTGTAAATTGGCT Reverse: GGATCTCAGGGTTGGGGTTG
Cd36	<i>Mus musculus</i>	Forward: AGATGACGTGGCAAAGAACAG Reverse: CCTTGGCTAGATAACGAACCTG
Fabp1	<i>Mus musculus</i>	Forward: ATGAACTTCTCCGGCAAGTAC Reverse: CTGACACCCCCTGATGTC
Fabp3	<i>Mus musculus</i>	Forward: ACCTGGAAGCTAGTGGACAG Reverse: TGATGGTAGTAGGTTGGTCAT
Fabp4	<i>Mus musculus</i>	Forward: AAGGTGAAGAGCATCATAACCC Reverse: TCACGCCTTTCATAACACATTCC
SCD1	<i>Mus musculus</i>	Forward: CCTCCGGAAATGAACGAGAG Reverse: CATCCTGATAGGTGGGGTCG
Elovl6	<i>Mus musculus</i>	Forward: GAAAAGCAGTTCAACGAGAACG Reverse: AGATGCCGACCACCAAAGATA
Acox1	<i>Mus musculus</i>	Forward: GCCAAGGCCACCTGAGTGAGC Reverse: ACCGCAAGGCCATCCGACATT
Acox2	<i>Mus musculus</i>	Forward: ACGGTCTGAACGCATTATG Reverse: TTGGCCCCATTAGCAATCTG
Cpt1	<i>Mus musculus</i>	Forward: GAACACAAATGTGCAAGCAGC Reverse: GCCATGACCGGCTTGATCTC
Cpt2	<i>Mus musculus</i>	Forward: CAGCACAGCATCGTACCCA Reverse: TCCCAATGCCGTTCTCAAAT
Ascl1	<i>Mus musculus</i>	Forward: CGATGGCTTGGACTTTGC Reverse: CACCCAGGCTCGACTGTATC
Acadl	<i>Mus musculus</i>	Forward: TCTTTCCTCGGAGCATGACA Reverse: GACCTCTACTCACTTCTCCAG
Acaa1a	<i>Mus musculus</i>	Forward: AGGCTCAAAGAACACCACCC Reverse: GGCTCCTGGCTAAGAACAT

Table 1.Continued

Name	Species	Sequence
Ehhadh	<i>Mus musculus</i>	Forward: CGGTCAATGCCATCAGTCCAA Reverse: TGCTCCACAGATCACTATGGC
ApoB	<i>Mus musculus</i>	Forward: GCTCAACTCAGGTTACCGTGA Reverse: AGGGTGTACTGGCAAGTTGG
MttP	<i>Mus musculus</i>	Forward: ATACAAGCTCACGTACTCCACT Reverse: TCTCTGTTGACCCGATTTTC
β -actin	<i>Mus musculus</i>	Forward: CATCGTAAAGACCTCTATGCCAAC Reverse: ATGGAGCCACCGATCCACA
Ch25h	<i>Rattus norvegicus</i>	Forward: GACCTGCATCACTCTCAGTT Reverse: TACAGTACATTGCTCTCCGG
LXR α	<i>Rattus norvegicus</i>	Forward: ACAACCCTGGGAGTGAGAG Reverse: TAGCATCCGTGGGAACAT
CYP7A1	<i>Rattus norvegicus</i>	Forward: CTGATGCTCCTGCTTGA Reverse: CTTCCAACCACGTATCAGTG
CYP27A1	<i>Rattus norvegicus</i>	Forward: AGTATGAGGTGGTCTGTCT Reverse: CAGCTGGTACTACTGTCTC
β -actin	<i>Rattus norvegicus</i>	Forward: CTTCTGCAGCTCCTCCGTC Reverse: CCTTCTGACCCATACCCACC
Ch25h	<i>Homo sapiens</i>	Forward: ACATGGAGTTCTCGTGTGG Reverse: CCCAGACGCTCATATACTGC
LXR α	<i>Homo sapiens</i>	Forward: TCTGGAGACATCTGGAGGTA Reverse: GGCCCCTGGAGAACTCGAAG
CYP7A1	<i>Homo sapiens</i>	Forward: TCCAGAAATCTACCCAGACC Reverse: GGCCCCTCTATAAGCTCCAAT
CYP27A1	<i>Homo sapiens</i>	Forward: GACATCCAACACGCTGACAT Reverse: AGTGGCAGAACACAAACTGG
ABCA1	<i>Homo sapiens</i>	Forward: AACTCTACATCTCCCTTCCCG Reverse: CTCCTGTGCGATGTCACTCC
β -actin	<i>Homo sapiens</i>	Forward: CATGTACGTTGCTATCCAGGC Reverse: CTCCCTTAATGTCACGCACGAT

ASBT, Apical sodium-dependent bile acid transporter; Ch25h, cholesterol 25-hydroxylase; CYP7A1, cytochrome P450 7A1; FGF15, fibroblast growth factor 15; IL, interleukin; LXR α , liver X receptor α ; MCP-1, monocyte chemoattractant protein 1; Shp, small heterodimer partner; TNF α , tumor necrosis factor α .

variance using the F test ($P > .05$). For data with normal distribution, the 2-tailed Student t test was used to compare 2 groups and 1-way analysis of variance with Bonferroni post-hoc test for multiple groups. For non-normally distributed data, the Mann-Whitney U test was used to compare 2 groups and Kruskal-Wallis with Dunn post hoc test for multiple groups. Data are expressed as mean \pm standard error of the mean, and differences were considered statistically significant at $P < .05$, whereas $P < .01$ and $P < .001$ represent more significant change.

References

- Michelotti GA, Machado MV, Diehl AM. NAFLD, NASH and liver cancer. *Nat Rev Gastroenterol Hepatol* 2013; 10:656–665.
- Rotman Y, Sanyal AJ. Current and upcoming pharmacotherapy for non-alcoholic fatty liver disease. *Gut* 2017; 66:180–190.
- Min HK, Kapoor A, Fuchs M, Mirshahi F, Zhou H, Maher J, Kellum J, Warnick R, Contos MJ, Sanyal AJ. Increased hepatic synthesis and dysregulation of cholesterol metabolism is associated with the severity of nonalcoholic fatty liver disease. *Cell Metab* 2012; 15:665–674.
- Ioannou GN. The role of cholesterol in the pathogenesis of NASH. *Trends Endocrinol Metab* 2016;27:84–95.
- Chiang JYL. Bile acid metabolism and signaling in liver disease and therapy. *Liver Res* 2017;1:3–9.
- Wang B, Tontonoz P. Liver X receptors in lipid signalling and membrane homeostasis. *Nat Rev Endocrinol* 2018; 14:452–463.
- Goodwin B, Watson MA, Kim H, Miao J, Kemper JK, Kliewer SA. Differential regulation of rat and human CYP7A1 by the nuclear oxysterol receptor liver X receptor-alpha. *Mol Endocrinol* 2003;17:386–394.
- Thomas C, Pellicciari R, Pruzanski M, Auwerx J, Schoonjans K. Targeting bile-acid signalling for metabolic diseases. *Nat Rev Drug Discov* 2008;7:678–693.
- Chow MD, Lee YH, Guo GL. The role of bile acids in nonalcoholic fatty liver disease and nonalcoholic steatohepatitis. *Mol Aspects Med* 2017;56:34–44.

10. de Aguiar Vallim TQ, Tarling EJ, Edwards PA. Pleiotropic roles of bile acids in metabolism. *Cell Metab* 2013; 17:657–669.
11. Qi Y, Jiang C, Cheng J, Krausz KW, Li T, Ferrell JM, Gonzalez FJ, Chiang JYL. Bile acid signaling in lipid metabolism: metabolomic and lipidomic analysis of lipid and bile acid markers linked to anti-obesity and anti-diabetes in mice. *Biochim Biophys Acta* 2015; 1851:19–29.
12. Li T, Owsley E, Matozel M, Hsu P, Novak CM, Chiang JYL. Transgenic expression of cholesterol 7alpha-hydroxylase in the liver prevents high-fat diet-induced obesity and insulin resistance in mice. *Hepatology* 2010;52:678–690.
13. Quintero P, Pizarro M, Solis N, Arab JP, Padilla O, Riquelme A, Arrese M. Bile acid supplementation improves established liver steatosis in obese mice independently of glucagon-like peptide-1 secretion. *J Physiol Biochem* 2014;70:667–674.
14. Gilat T, Leikin-Frenkel A, Goldiner I, Juhel C, Lafont H, Gobbi D, Konikoff FM. Prevention of diet-induced fatty liver in experimental animals by the oral administration of a fatty acid bile acid conjugate (FABAC). *Hepatology* 2003;38:436–442.
15. Ferrell JM, Boehme S, Li F, Chiang JYL. Cholesterol 7alpha-hydroxylase-deficient mice are protected from high-fat/high-cholesterol diet-induced metabolic disorders. *J Lipid Res* 2016;57:1144–1154.
16. Zhao J, Chen J, Li M, Chen M, Sun C. Multifaceted functions of CH25H and 25HC to modulate the lipid metabolism, immune responses, and broadly antiviral activities. *Viruses* 2020;12:727.
17. Adams CM, Reitz J, De Brabander JK, Feramisco JD, Li L, Brown MS, Goldstein JL. Cholesterol and 25-hydroxycholesterol inhibit activation of SREBPs by different mechanisms, both involving SCAP and Insigs. *J Biol Chem* 2004;279:52772–52780.
18. Cyster JG, Dang EV, Rebaldi A, Yi T. 25-Hydroxycholesterols in innate and adaptive immunity. *Nat Rev Immunol* 2014;14:731–743.
19. Yan R, Cao P, Song W, Qian H, Du X, Coates HW, Zhao X, Li Y, Gao S, Gong X, Liu X, Sui J, Lei J, Yang H, Brown AJ, Zhou Q, Yan C, Yan N. A structure of human Scap bound to Insig-2 suggests how their interaction is regulated by sterols. *Science* 2021;371:eabb2224.
20. Zang R, Case JB, Yutuc E, Ma X, Shen S, Gomez Castro MF, Liu Z, Zeng Q, Zhao H, Son J, Rothlauf PW, Kreutzberger AJB, Hou G, Zhang H, Bose S, Wang X, Vahey MD, Mani K, Griffiths WJ, Kirchhausen T, Fremont DH, Guo H, Diwan A, Wang Y, Diamond MS, Whelan SPJ, Ding S. Cholesterol 25-hydroxylase suppresses SARS-CoV-2 replication by blocking membrane fusion. *Proc Natl Acad Sci U S A* 2020; 117:32105–32113.
21. Wang S, Li W, Hui H, Tiwari SK, Zhang Q, Croker BA, Rawlings S, Smith D, Carlin AF, Rana TM. Cholesterol 25-hydroxylase inhibits SARS-CoV-2 and other coronaviruses by depleting membrane cholesterol. *EMBO J* 2020;39:e106057.
22. Noebauer B, Jais A, Todoric J, Gossens K, Sutterluty-Fall H, Einwallner E. Hepatic cholesterol-25-hydroxylase overexpression improves systemic insulin sensitivity in mice. *J Diabetes Res* 2017;2017:4108768.
23. Li D, Wang X, Ren W, Ren J, Lan X, Wang F, Li H, Zhang F, Han Y, Song T, Holmdahl R, Lu S. High expression of liver histone deacetylase 3 contributes to high-fat-diet-induced metabolic syndrome by suppressing the PPAR-gamma and LXR-alpha-pathways in E3 rats. *Mol Cell Endocrinol* 2011;344:69–80.
24. Gao Q, Jia Y, Yang G, Zhang X, Boddu PC, Petersen B, Narsingam S, Zhu YJ, Thimmapaya B, Kanwar YS, Reddy JK. PPARalpha-deficient ob/ob obese mice become more obese and manifest severe hepatic steatosis due to decreased fatty acid oxidation. *Am J Pathol* 2015;185:1396–1408.
25. Li-Hawkins J, Gafvels M, Olin M, Lund EG, Andersson U, Schuster G, Bjorkhem I, Russell DW, Eggertsen G. Cholic acid mediates negative feedback regulation of bile acid synthesis in mice. *J Clin Invest* 2002;110:1191–1200.
26. Rebaldi A, Dang EV, McDonald JG, Liang G, Russell DW, Cyster JG. Inflammation. 25-Hydroxycholesterol suppresses interleukin-1-driven inflammation downstream of type I interferon. *Science* 2014;345:679–684.
27. Peet DJ, Turley SD, Ma W, Janowski BA, Lobaccaro JM, Hammer RE, Mangelsdorf DJ. Cholesterol and bile acid metabolism are impaired in mice lacking the nuclear oxysterol receptor LXR alpha. *Cell* 1998;93:693–704.
28. Lehmann JM, Kliewer SA, Moore LB, Smith-Oliver TA, Oliver BB, Su JL, Sundseth SS, Winegar DA, Blanchard DE, Spencer TA, Willson TM. Activation of the nuclear receptor LXR by oxysterols defines a new hormone response pathway. *J Biol Chem* 1997; 272:3137–3140.
29. Chen JY, Levy-Wilson B, Goodart S, Cooper AD. Mice expressing the human CYP7A1 gene in the mouse CYP7A1 knock-out background lack induction of CYP7A1 expression by cholesterol feeding and have increased hypercholesterolemia when fed a high fat diet. *J Biol Chem* 2002;277:42588–42595.
30. Kim I, Ahn SH, Inagaki T, Choi M, Ito S, Guo GL, Kliewer SA, Gonzalez FJ. Differential regulation of bile acid homeostasis by the farnesoid X receptor in liver and intestine. *J Lipid Res* 2007;48:2664–2672.
31. Wahlstrom A, Kovatcheva-Datchary P, Stahlman M, Backhed F, Marschall HU. Crosstalk between bile acids and gut microbiota and its impact on farnesoid X receptor signalling. *Dig Dis* 2017;35:246–250.
32. Streidl T, Karkossa I, Segura Munoz RR, Eberl C, Zaufel A, Plagge J, Schmaltz R, Schubert K, Basic M, Schneider KM, Afify M, Trautwein C, Tolba R, Stecher B, Doden HL, Ridlon JM, Ecker J, Moustafa T, von Bergen M, Ramer-Tait AE, Clavel T. The gut bacterium *Extibacter muris* produces secondary bile acids and influences liver physiology in gnotobiotic mice. *Gut Microbes* 2021;13:1–21.
33. Jiang C, Xie C, Li F, Zhang L, Nichols RG, Krausz KW, Cai J, Qi Y, Fang ZZ, Takahashi S, Tanaka N, Desai D,

- Amin SG, Albert I, Patterson AD, Gonzalez FJ. Intestinal farnesoid X receptor signaling promotes nonalcoholic fatty liver disease. *J Clin Invest* 2015;125:386–402.
34. Li Z, Martin M, Zhang J, Huang HY, Bai L, Zhang J, Kang J, He M, Li J, Maurya MR, Gupta S, Zhou G, Sangwung P, Xu YJ, Lei T, Huang HD, Jain M, Jain MK, Subramaniam S, Shyy JY. Kruppel-like factor 4 regulation of cholesterol-25-hydroxylase and liver X receptor mitigates atherosclerosis susceptibility. *Circulation* 2017;136:1315–1330.
35. Neuschwander-Tetri BA, Loomba R, Sanyal AJ, Lavine JE, Van Natta ML, Abdelmalek MF, Chalasani N, Dasarathy S, Diehl AM, Hameed B, Kowdley KV, McCullough A, Terrault N, Clark JM, Tonascia J, Brunt EM, Kleiner DE, Doo E; NASH Clinical Research Network. Farnesoid X nuclear receptor ligand obeticholic acid for non-cirrhotic, non-alcoholic steatohepatitis (FLINT): a multicentre, randomised, placebo-controlled trial. *Lancet* 2015;385:956–965.
36. Ratiu V, Harrison SA, Francque S, Bedossa P, Lehert P, Serfaty L, Romero-Gomez M, Boursier J, Abdelmalek M, Caldwell S, Drenth J, Anstee QM, Hum D, Hanf R, Roudot A, Megnien S, Staels B, Sanyal A. GOLDEN-505 Investigator Study Group. Elafibranor, an agonist of the peroxisome proliferator-activated receptor-alpha and -delta, induces resolution of nonalcoholic steatohepatitis without fibrosis worsening. *Gastroenterology* 2016;150:1147–1159.e5.
37. Anstee QM, Neuschwander-Tetri BA, Wong VW, Abdelmalek MF, Younossi ZM, Yuan J, Pecoraro ML, Seyedkazemi S, Fischer L, Bedossa P, Goodman Z, Alkhouri N, Tacke F, Sanyal A. Cenicriviroc for the treatment of liver fibrosis in adults with nonalcoholic steatohepatitis: AURORA Phase 3 study design. *Contemp Clin Trials* 2020;89:105922.
38. Kazankov K, Jorgensen SMD, Thomsen KL, Moller HJ, Vilstrup H, George J, Schuppan D, Gronbaek H. The role of macrophages in nonalcoholic fatty liver disease and nonalcoholic steatohepatitis. *Nat Rev Gastroenterol Hepatol* 2019;16:145–159.
39. Wang X, Guo M, Wang Q, Wang Q, Zuo S, Zhang X, Tong H, Chen J, Wang H, Chen X, Guo J, Su X, Liang H, Zhou H, Li JZ. The patatin-like phospholipase domain containing protein 7 facilitates VLDL secretion by modulating ApoE stability. *Hepatology* 2020;72:1569–1585.
40. Bai L, Jia Y, Viswakarma N, Huang J, Vluggens A, Wolins NE, Jafari N, Rao MS, Borensztajn J, Yang G, Reddy JK. Transcription coactivator mediator subunit MED1 is required for the development of fatty liver in the mouse. *Hepatology* 2011;53:1164–1174.
41. Huang da W, Sherman BT, Lempicki RA. Systematic and integrative analysis of large gene lists using DAVID bioinformatics resources. *Nat Protoc* 2009;4:44–57.
42. Huang da W, Sherman BT, Lempicki RA. Bioinformatics enrichment tools: paths toward the comprehensive functional analysis of large gene lists. *Nucleic Acids Res* 2009;37:1–13.

Received September 24, 2021. Accepted December 28, 2021.

Correspondence

Address correspondence to: Liang Bai, PhD, Institute of Cardiovascular Science, Translational Medicine Institute, Xi'an Jiaotong University Health Science Center, Xi'an, Shaanxi 710061, China. e-mail: baijiang0922@mail.xjtu.edu.cn; tel: 86 298 265 5363; fax: 86 298 265 5362. or John Y-J. Shyy, PhD, Department of Medicine/Division of Cardiology, University of California, San Diego, 9500 Gilman Dr, La Jolla, CA 92093. e-mail: jshyy@health.ucsd.edu; tel: (858) 534-3737.

Acknowledgement

The authors thank Prof Shemin Lu (Xi'an Jiaotong University, China) and Dr Jiansheng Huang (Washington University, St Louis, MO) for their constructive suggestions to our studies. We thank the Laboratory Animal Center of Xi'an Jiaotong University for animal technical support.

CRedit Authorship Contribution

Zeyu Dong (Formal analysis: Lead; Investigation: Lead; Methodology: Lead; Project administration: Lead; Resources: Lead; Validation: Lead; Writing – original draft: Supporting)

Fangzhou He (Data curation: Equal; Formal analysis: Lead; Methodology: Equal)

Xiaosong Yan (Data curation: Lead; Formal analysis: Equal; Methodology: Equal; Validation: Lead)

Yuanming Xing (Formal analysis: Equal; Methodology: Supporting; Visualization: Lead)

Yuyang Lei (Formal analysis: Lead; Methodology: Supporting)

Jie Gao (Methodology: Supporting; Validation: Equal)

Ming He (Conceptualization: Equal; Project administration: Equal; Supervision: Supporting)

Dongmin Li (Funding acquisition: Supporting; Resources: Supporting; Writing – review & editing: Supporting)

Liang Bai (Conceptualization: Lead; Funding acquisition: Equal; Project administration: Lead; Supervision: Lead; Writing – original draft: Lead)

Zuyi Yuan (Funding acquisition: Equal; Resources: Equal; Supervision: Supporting; Writing – review & editing: Supporting)

John Y-J. Shyy (Conceptualization: Lead; Funding acquisition: Lead; Project administration: Lead; Writing – review & editing: Lead)

Conflicts of interest

The authors disclose no conflicts.

Funding

This work was supported by grants from the National Natural Science Foundation of China (82070470 to L.B.; 92049203, 81941005 to Z.Y.Y.; 81770864 to D.M.L.), the National Key R&D Program of China (2021YFA1301200, 2019YFA0802300), and China Postdoctoral Science Foundation Grant (2020M673424, 2021T140541 to L.B.).